cmgh
CELLULAR AND MOLECULAR GASTROENTEROLOGY AND HEPATOLOGY

ORIGINAL RESEARCH

Modulation of Cancer-Associated Fibrotic Stroma by An Integrin $\alpha_v\beta_3$ Targeting Protein for Pancreatic Cancer Treatment

Ravi Chakra Turaga,[1,*] Malvika Sharma,[1,*] Falguni Mishra,[1] Alyssa Krasinskas,[2] Yi Yuan,[1] Jenny J. Yang,[3] Shiyuan Wang,[4] Chunfeng Liu,[4] Sun Li,[4] and Zhi-Ren Liu[1]

[1]Department of Biology, [3]Department of Chemistry, Georgia State University, Atlanta, Georgia; [2]Department of Pathology, Emory University, Atlanta, Georgia; [4]Research and Development Division, Amoytop Biotech, Inc, Xiamen, People's Republic of China

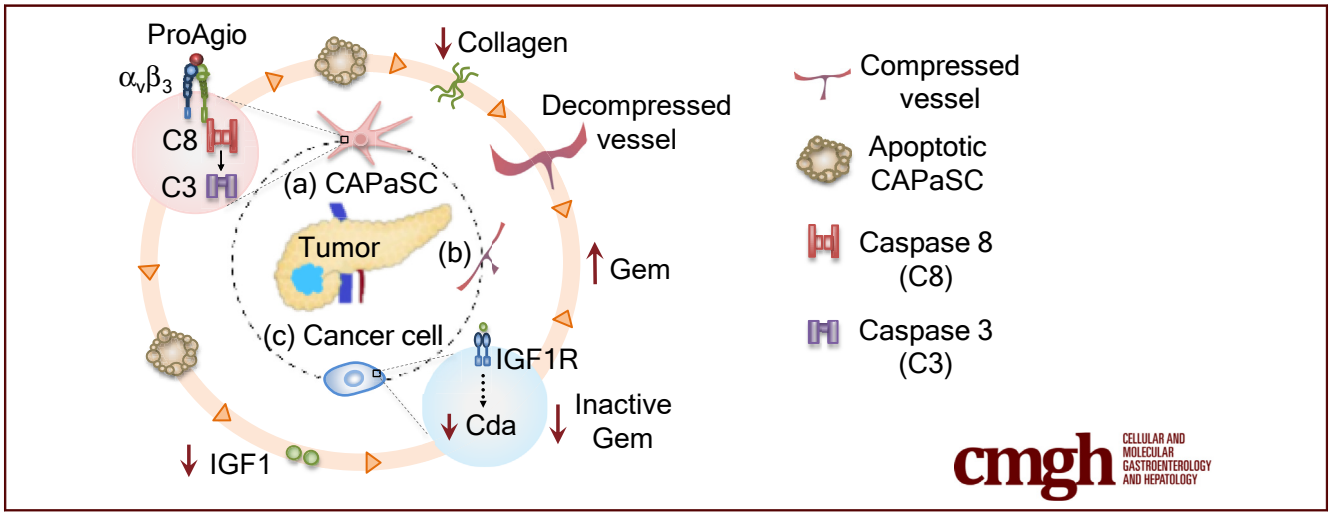

SUMMARY

Dense stroma is a major obstacle in the treatment of pancreatic ductal adenocarcinoma. By using a de novo–designed protein agent (ProAgio) that induces cell apoptosis by targeting integrin $\alpha_v\beta_3$, we show an effective approach for pancreatic ductal adenocarcinoma treatment by simultaneously targeting cancer–associated pancreatic stellate cells and angiogenic endothelial cells.

BACKGROUND & AIMS: Pancreatic ductal adenocarcinoma (PDAC) is resistant to most therapeutics owing to dense fibrotic stroma orchestrated by cancer-associated pancreatic stellate cells (CAPaSC). CAPaSC also support cancer cell growth, metastasis, and resistance to apoptosis. Currently, there is no effective therapy for PDAC that specifically targets CAPaSC. We previously reported a rationally designed protein, ProAgio, that targets integrin $\alpha_v\beta_3$ at a novel site and induces apoptosis in integrin $\alpha_v\beta_3$-expressing cells. Because both CAPaSC and angiogenic endothelial cells express high levels of integrin $\alpha_v\beta_3$, we aimed to analyze the effects of ProAgio in PDAC tumor.

METHODS: Expression of integrin $\alpha_v\beta_3$ was examined in both patient tissue and cultured cells. The effects of ProAgio on CAPaSC were analyzed using an apoptosis assay kit. The effects of ProAgio in PDAC tumor were studied in 3 murine tumor models: subcutaneous xenograft, genetic engineered ($Kras^{G12D}$; $p53^{R172H}$; Pdx1-Cre, GEM-KPC) mice, and an orthotopic KrasG12D; p53R172H; Pdx1-Cre (KPC) model.

RESULTS: ProAgio induces apoptosis in CAPaSC. ProAgio treatment significantly prolonged survival of a genetically engineered mouse–KPC and orthotopic KPC mice alone or in combination with gemcitabine (Gem). ProAgio specifically induced apoptosis in CAPaSC, resorbed collagen, and opened collapsed tumor vessels without an increase in angiogenesis in PDAC tumor, enabling drug delivery into the tumor. ProAgio decreased intratumoral insulin-like growth factor 1 levels as a result of depletion of CAPaSC and consequently decreased cytidine deaminase, a Gem metabolism enzyme in cancer cells, and thereby reduced resistance to Gem-induced apoptosis.

CONCLUSIONS: Our study suggests that ProAgio is an effective PDAC treatment agent because it specifically depletes CAPaSC and eliminates tumor angiogenesis, thereby enhancing drug delivery and Gem efficacy in PDAC tumors. *(Cell Mol Gastroenterol Hepatol 2021;11:161–179; https://doi.org/10.1016/j.jcmgh.2020.08.004)*

Keywords: Pancreatic Cancer Treatment; Pancreatic Stellate Cells; Integrin $\alpha_v\beta_3$; Collagen; Gemcitabine.

Pancreatic ductal adenocarcinoma (PDAC) is one of the most lethal diseases, with a median survival of fewer than 6 months after diagnosis. Despite intensive

efforts in developing effective treatments, patient survival has improved only marginally. Dense fibrotic stroma and extracellular matrix laid down by cancer-associated pancreatic stellate cells (CAPaSC) is considered to be one of the major contributors to resistance to antitumor therapies in this disease.[1–3] CAPaSC also engage in symbiotic growth factor and cytokine cross-talk with cancer cells that support tumor growth, survival, resistance to apoptosis, and metastasis.[4–7] In return, cancer cells provide factors that support PaSC proliferation and survival. Prior studies have shown that depleting cancer-associated fibroblasts (CAFs) and fibrosis can improve the efficacy of existing PDAC treatments in preclinical models.[1,3] However, recent studies of Sonic hedgehog (Shh) and α-smooth muscle actin (α-SMA) gene deletion in genetically engineered mouse (GEM) models of PDAC have suggested that some fibrotic stroma in PDAC may constitute a barrier that prevents metastatic spread of the tumor.[8–10] Depletion of fibrotic stroma results in increased metastasis and shorter survival in preclinical models and some early phase clinical studies.[8,9,11] These studies caused a very important controversy, "target or not-target fibrotic stroma in cancer therapies, particularly in treatment of PDAC?"[12]

Integrin $\alpha_v\beta_3$ is not expressed, or is expressed at very low levels, in most normal tissues/cells. However, high levels of integrin $\alpha_v\beta_3$ often are detected in tissues at inflammatory sites, wound healing, and invasive cancers. The integrin is highly expressed in angiogenic endothelial cells and collagen-secreting myofibroblasts. Because of a lack of expression in most normal tissues/cells, it is believed that this integrin pair is an ideal and safe target for drug development for multiple pathologic conditions.[13–15] We previously reported the development of a rationally designed protein (ProAgio) that targets integrin $\alpha_v\beta_3$ at a novel site. ProAgio effectively induces apoptosis in $\alpha_v\beta_3$-expressing cells.[16] It previously was shown that activated hepatic stellate cells express high levels of integrin $\alpha_v\beta_3$.[17–19] PaSC share very similar properties with hepatic stellate cells,[20] which prompted us to question whether activation of PaSC leads to higher expression of integrin $\alpha_v\beta_3$, thus constituting an ideal target for ProAgio. We show here that activated PaSC and CAPaSC in PDAC tumors express high levels of integrin $\alpha_v\beta_3$. By targeting integrin $\alpha_v\beta_3$, ProAgio is effective in inducing apoptosis of the activated PaSC and CAPaSC. By simultaneously targeting CAPaSC and angiogenic endothelial cells, ProAgio is effective for PDAC treatment. ProAgio depletes CAPaSC, resorbs tumor collagen, and abrogates angiogenic vessels in PDAC tumor. ProAgio treatment leads to the opening of collapsed tumor vessels, which increases tumor permeability, and facilitates drug delivery. Importantly, depletion of CAPaSC by ProAgio also reduces various growth factors and cytokines that are released from CAPaSC, and therefore breaks down the cross-talk between CAPaSC and cancer cells. As an example, ProAgio decreases insulin-like growth factor 1 (IGF1) in the tumor. A decrease in IGF1 consequently decreases cytidine deaminase (Cda) in PDAC tumor, thereby resulting in much enhanced gemcitabine efficacy in addition to an increase in the drug delivery. We conclude that specifically targeting CAPaSC by ProAgio, leaving the normal or quiescent PaSC intact, may provide an important treatment advantage.

Results

CAPaSC Express High Levels of Integrin $\alpha_v\beta_3$ and ProAgio Induces CAPaSC Apoptosis

To examine whether the integrin $\alpha_v\beta_3$ also is expressed in PaSC and CAPaSC, we first probed integrin $\alpha_v\beta_3$ levels in activated/inactivated human primary PaSC. Integrin $\alpha_v\beta_3$ is highly expressed in activated PaSC. However, inactivated PaSC expressed little to no integrin $\alpha_v\beta_3$ (Figure 1*A*). To evaluate the expression of integrin $\alpha_v\beta_3$ in PaSC in PDAC, we analyzed PDAC patient tumor tissues for the expression of integrin β_3. We found that integrin β_3 was highly upregulated in PDAC tumor tissues. The integrin expression was particularly high in the stromal component as compared with the areas of the tumor with histologically evident adenocarcinoma. Immunostaining also showed that CAPaSC showed higher integrin β_3 expression, although there was almost no integrin β_3 staining in noncancerous tissues (Figure 1*B*). Consistently, survival analyses of PDAC patients with high and low integrin α_v, integrin β_3, and α-SMA expression in tumors from the KM-plotter data base[21] showed that integrin $\alpha_v\beta_3$ and α-SMA levels in tumor closely correlate with poor patient overall survival and relapse-free survival (Figure 1*C* and *D*), indicating the important role of integrin $\alpha_v\beta_3$-expressing cells and α-SMA–positive cells in cancer progression and patient response to treatment. ProAgio induces apoptosis in $\alpha_v\beta_3$-expressing cells.[16] We reasoned whether ProAgio could exert its effect on activated PaSC. Clearly, ProAgio effectively induced apoptosis in activated human primary PaSC, whereas it had a minimal effect on inactivated PaSC (Figure 1*E*). Similar to our previous observation,[16] ProAgio induced apoptosis in activated PaSC by recruiting and activating caspase 8 at the intracellular domain of the integrin β_3 (Figure 1*F*). Our findings suggest that targeting integrin $\alpha_v\beta_3$ by ProAgio may be a unique approach that is capable of specifically depleting CAPaSC in PDAC to facilitate treatment.

Targeting Integrin $\alpha_v\beta_3$ by ProAgio Inhibits Tumor Growth and Provides a Survival Benefit

To test the conjecture, we first examined the effects of ProAgio in mice bearing subcutaneous xenograft tumors established by co-implanting activated human PaSC with

***Authors share co-first authorship.**

Abbreviations used in this paper: **α-SMA, α smooth muscle actin; CAF, cancer-associated fibroblast; CAPaSC, cancer-associated pancreatic stellate cells; Cda, cytidine deaminase; Dck, deoxycytidine kinase; dFDC, 2′,2′-difluorodeoxcytidine; dFdCTP, gemcitabine triphosphate; dFdU, 2′,2′-difluorodeoxyuridine; Gem, gemcitabine; GEM, genetically engineered mouse; IGF1, insulin-like growth factor 1; IGF1R, Insulin-like growth factor 1 receptor; KPC, LSL-Kras$^{G12D/+}$;LSL-Trp53$^{R172H/+}$;Pdx-1-Cre; LSL, Lox-Stop-Lox; mRNA, messenger RNA; OrKPC, KPC 961 cell line; PDAC, pancreatic ductal adenocarcinoma; Shh, Sonic hedgehog; Tdk, Thymidine kinase.**

Most current article

2352-345X
https://doi.org/10.1016/j.jcmgh.2020.08.004

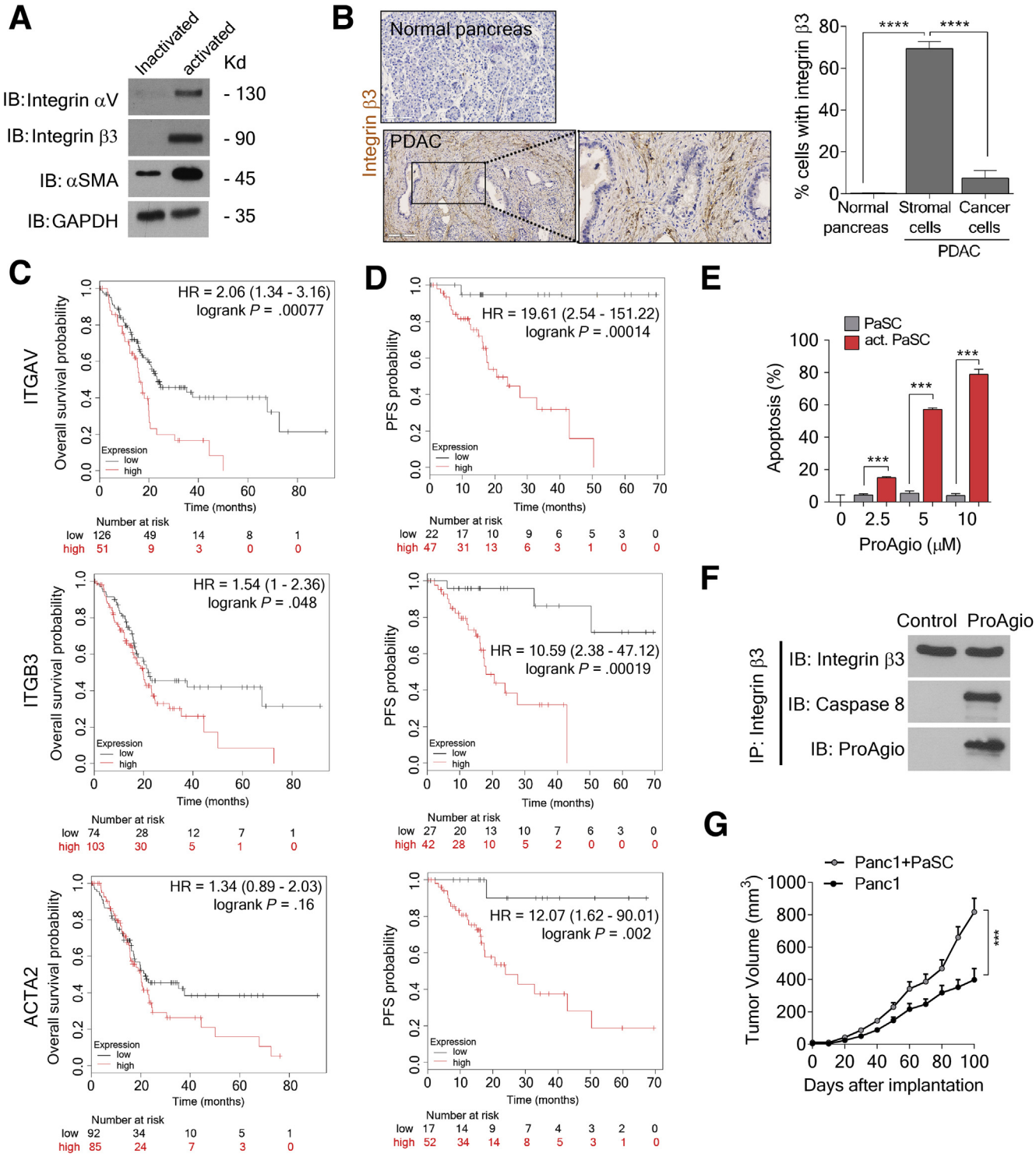

human Panc1 cells. Co-implantation with human PaSC significantly promoted tumor growth (Figure 1*G*). ProAgio inhibited Panc-1 tumor growth without PaSC co-implant, although the inhibitory effects were greater when Panc1 was co-implanted with human PaSC (Figure 2*A*). Consistently, tumors in mice in the ProAgio treatment group weighed less at the end of the experiment compared with the vehicle group (Figure 2*B*). Upon activation, PaSC attain a myofibroblast-like phenotype, up-regulating α-SMA and integrin $\alpha_v\beta_3$, and secrete collagen. Because ProAgio effectively induced apoptosis in activated PaSC, we reasoned whether ProAgio would exert its effects in vivo on co-

implanted PaSC, and thus on the collagen secreted by the PaSC. Immunostain showed that α-SMA–positive cells were reduced with much higher reduction in the PaSC co-implanted tumors (Figure 2*C* and *D*), and Masson trichrome stain showed a decrease in intratumoral collagen content after ProAgio treatment (Figure 2*E* and *F*). The co-implanted PaSC facilitated Panc1 proliferation in tumor as shown by increased Ki67 staining. ProAgio abrogated the effects of tumor proliferation promoted by PaSC (Figure 2*G* and *H*). Similar to our previous observation, ProAgio treatment decreased the tumor vasculature (Figure 2*I* and *J*).

It is noteworthy that the Panc1 subcutaneous xenograft model does not recapitulate some important properties of patient PDAC tumors, especially the dense fibrotic stroma and the collapsed intratumoral vessels. To accurately evaluate the effects of depletion of CAPaSC by ProAgio on PDAC, we used a GEM model: Lox-Stop-Lox (LSL)-$Kras^{G12D/+}$;LSL-$Trp53^{R172H/+}$;Pdx-1-Cre (KPC) (referred to as GEM-KPC)[1,22] (Figure 3*A* and *B*). The ProAgio single agent modestly prolonged GEM-KPC mice survival (Figure 3*C*). An orthotopic model of PDAC is another model system that well-mimics the patient PDAC tumor microenvironment. In addition, owing to rapid growth of the tumor,[23] the orthotopic model is excellent to test the treatment effects of drug on PDAC. Thus, the effectiveness of ProAgio on PDAC also was tested in mice bearing orthotopic tumors derived from cells isolated from the tumor of KPC mice (KPC 961 cell line,[24] referred to as OrKPC hereafter). ProAgio provided significant survival benefit compared with vehicle (Figure 3*D*). Analyses of tumor sections from GEM-KPC and OrKPC mice at the end of the survival experiment or immediately after 20 doses of ProAgio treatment showed a significant reduction in the levels of fibrosis, as shown by reduced intratumoral collagen content (Figure 3*E*, *F*, and *H*), and levels of α-SMA–positive fibroblasts (Figure 3*E*, *G*, and *H*). In consistence, messenger RNA (mRNA) levels of α-SMA and Fibroblast activation protein (FAP) measured by quantitative reverse-transcription polymerase chain reaction were reduced significantly in the tumor lysates of GEM-KPC mice upon treatment with ProAgio (Figure 3*I*), suggesting a reduction in CAPaSC by ProAgio in the tumor. We previously showed that ProAgio shows anti-angiogenic activity resulting from induction of apoptosis in angiogenic endothelial cells.[16] We therefore analyzed the effects of ProAgio on tumor vessels in the treated GEM-KPC and OrKPC tumors. Unlike previous observations that depletion of cancer-associated fibroblasts by genetically depleting the *Shh* gene promotes tumor angiogenesis,[1] depletion of CAPaSC by ProAgio did not result in an increase of vessel density in both GEM-KPC and OrKPC tumors (Figure 4*A*, *B*, *E*, and *F*). However, ProAgio treatment showed a profound effect on the tumor vasculature because the majority of intratumoral vessels were noted to be prominently open and, when measured, the mean vessel luminal area was increased significantly (Figure 4*A*, *C*, *E*, and *G*). A similar phenomenon also was observed and reported by Olive et al.[1] This is presumably owing to relief of high intratumoral pressure because of depleted rigid and dense collagen fibrils.

Depletion of CAPaSC by ProAgio Increases Intratumoral Drug Delivery

One of the major reasons for chemoresistance in PDAC is the impediment of drug delivery owing to the presence of dense collagen fibrils that physically block drug distribution inside the tumor and the completely collapsed intratumoral blood vessels that lead to poor blood perfusion.[25,26] ProAgio reduced tumor collagen and opened the intratumoral vessels without an increase in angiogenesis. We therefore believed that ProAgio could eliminate both drug delivery barriers and thereby facilitate the delivery of chemotherapeutic agents to tumor. To evaluate the effects of ProAgio on drug delivery, GEM-KPC mice were treated with 8 daily doses of ProAgio, followed by 1 intravenous dose of gemcitabine (Gem). Tumor lysates subsequently were analyzed. ProAgio treatment resulted in a more than 2.5-fold increase in intratumoral Gem delivery (Figure 4*D*). A similar increase also was observed in ProAgio-treated OrKPC mice upon intravenous administration of fluorescent probe–conjugated

Figure 1. (***See previous page***). **CAPaSC express integrin $\alpha_v\beta_3$. ProAgio induces CAPaSC apoptosis.** (*A*) Levels of αV (IB, integrin αV) and β3 (IB, integrin β3) integrin in activated and inactivated human primary PaSC were analyzed by immunoblot. PaSC were activated by culturing for 48 hours in the presence of 5 ng/mL transforming growth factor (TGF)-β. Inactivated PaSC are the cells that are in day 1 culture without TGF-β. (*B*) (*Left*) Representative (tissue samples from 9 patients and a tissue array of 60 patients) images and (*right*) quantification of integrin β_3-positive cells in stromal and adenocarcinoma (cancer cells) areas of the IHC staining of integrin β_3 of PDAC patient tumor tissue samples (n = 69). (*C* and *D*) Overall survival (*C*) and relapse-free survival (*D*) of PDAC patients in the groups of high and low expression of integrin αv (ITGAV, *top*), integrin β_3 (ITGB3, *middle*), and α-SMA (ACTA2, *bottom*) were plotted from the KM-plotter data base. ITGAV, ITGB3, and ACTA2 expression high (*red line*) denotes that the mRNA levels of the gene in the tumor of the patients are higher than the median value of mRNA of the gene in the entire patient group, and expression low (*black line*) is defined by the mRNA levels of the gene in the tumor of the patients are lower than the median value of the mRNA of the gene in the entire patient group. The number at the bottom of each panel indicates patient number. The hazard ratio (HR) and log-rank *P* value are indicated in each panel. (*E*) Apoptosis in activated PaSC (act. PaSC, *red bar*) or inactivated (PaSC, *grey bar*) PaSC after treatment with the indicated concentrations of ProAgio was measured by an apoptosis kit. Cell apoptosis is presented as the percentage of apoptosis by defining the apoptosis of untreated cells as 0%. (*F*) Co-immunoprecipitation of caspase 8 with integrin β_3 (IP, integrin β_3) in extracts of activated human primary PaSC that were treated with 5 μmol/L ProAgio for 6 hours were analyzed by immunoblots (IB, caspase 8). Immunoblot of integrin β_3 (IB, integrin β_3) indicates the amount of β_3 precipitated down in the co-IP. Immunoblot of ProAgio (IB, ProAgio) indicates co-precipitation of ProAgio with integrin β_3. (*G*) Mean tumor volume of subcutaneous xenograft of Panc1 with (*gray line*, Panc1 + CAPaSC) or without (*black line*, Panc1) co-implantation of PaSC. (*B*, *E*, and *G*) Error bars represent means ± SEM. GAPDH, glyceraldehyde-3-phosphate dehydrogenase. **P* < .05; ***P* < .01; ****P* < .001; *****P* < .0001. co-IP, co-immunoprecipitation; IB, immunoblot; IP, immunoprecipitation; n.s., denotes not significant.

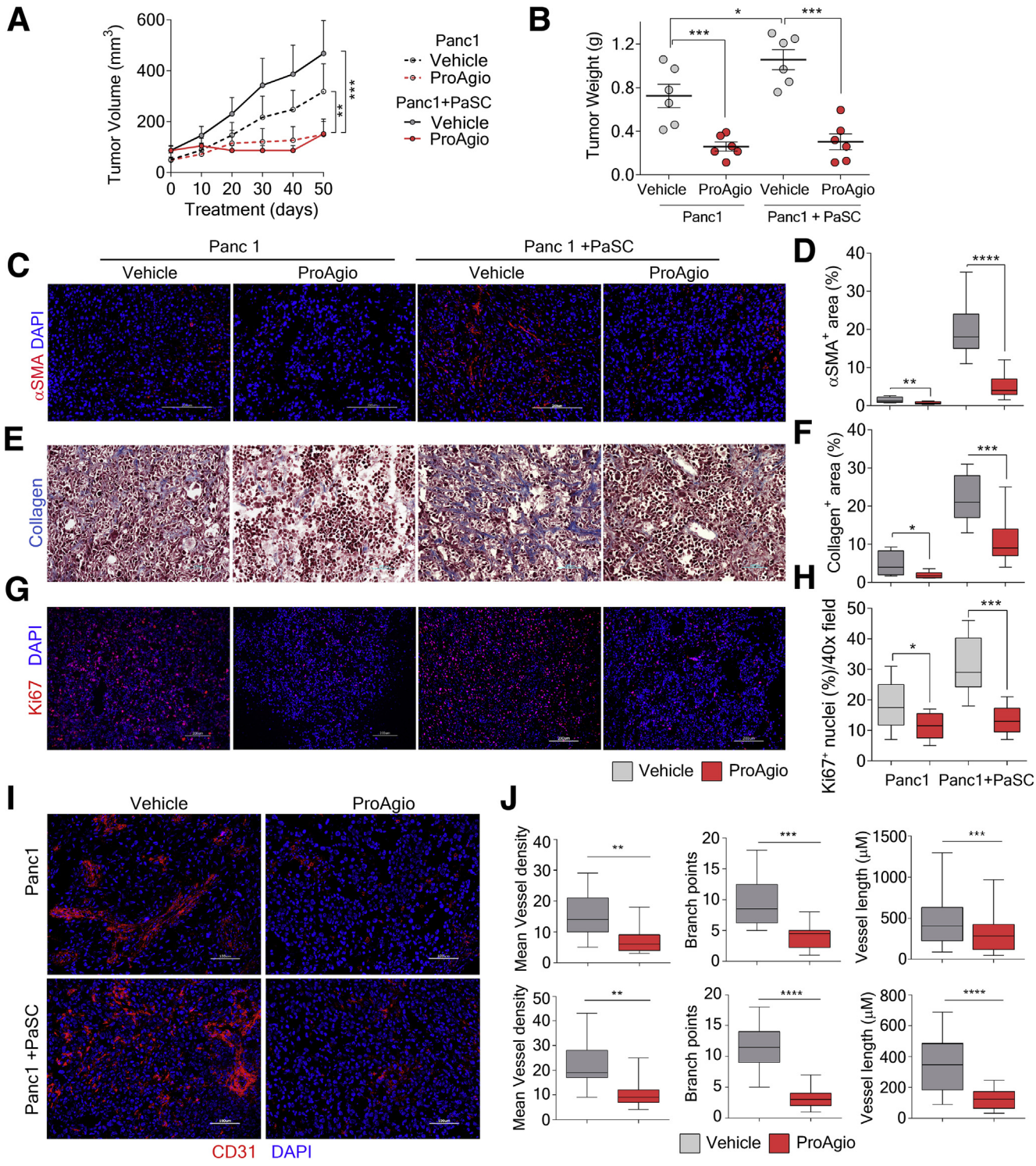

molecules (paclitaxel and IgG) after 8 daily doses of ProAgio (Figure 4*H* and *I*).

A strong increase in drug molecule intratumoral delivery predicts the treatment efficacy of ProAgio in combination with other anticancer drugs. We performed treatment using ProAgio in combination with Gem (50 mg/kg intraperitoneally twice weekly) in both GEM-KPC and OrKPC models. The treatment started at a late stage of cancer development (Figure 5*A* and *B*). In the GEM-KPC model, Gem alone provided a marginal survival benefit, ProAgio alone provided a modest survival benefit, and ProAgio combined with Gem dramatically prolonged GEM-KPC mice survival

(Figure 5*C*). Similar results were observed in the OrKPC model (Figure 5*D*). An increase in apoptosis in the stromal area was observed in the ProAgio group, although this increase was not observed in the Gem group (Figure 5*F*). ProAgio alone did not lead to a substantial increase in apoptosis in areas of histologically evident adenocarcinoma in the tumor. A more than 3-fold increase in apoptosis in the adenocarcinoma area was observed in the ProAgio and Gem combination group compared with the ProAgio alone group (Figure 5*G*), suggesting that ProAgio induced apoptosis in stromal fibroblasts, although it had less effects on PDAC cancer cells. In case of the combination, ProAgio increased the delivery of Gem, which led to cancer cell apoptosis. The observation was consistent with in vitro tests with PDAC cancer cells and PaSC (Figure 5*H*). In addition, the combination of ProAgio and Gem did not have an additive effect on cultured pancreatic cancer cells (Figure 5*I*). We measured the collagen content and levels of α-SMA–positive cells in the treated tumors. Both ProAgio and ProAgio plus Gem reduced intratumoral collagen content and α-SMA–positive cells in GEM-KPC (Figure 6*A*–*C* and *E*) and OrKPC tumors (Figure 6*A*, *B*, *D*, and *F*). Because of a reduction in intratumoral collagen, ProAgio and ProAgio plus Gem treatments resulted in reduced tumor weight (Figure 5*E*). We again analyzed delivery of the fluorescence probe–conjugated paclitaxel and IgG to the tumors under ProAgio and ProAgio plus Gem. Interestingly, the ProAgio plus Gem combination further increased the drug molecule delivery dramatically (Figure 4*J*–*L*) compared with ProAgio alone. Although we do not understand the molecular mechanism by which ProAgio plus Gem further increases tumor permeability, such a drastic increase in intratumoral delivery of drug molecule would confer a good treatment benefit.

Depletion of CAPaSC by ProAgio Enhances Gem Efficacy by Altering Gem Metabolism

ProAgio plus Gem offers a strong survival benefit over Gem or ProAgio alone. We sought to elucidate the mechanism(s) that may contribute to such strongly enhanced antitumor activity of the combination therapy. We examined the intratumoral levels of the Gem prodrug 2′,2′-difluorodeoxycytidine (dFdC) and the inactivated and activated metabolites (2′,2′-difluorodeoxyuridine [dFdU] and gemcitabine triphosphate [dFdCTP]).[27–29] We found that the combination led to a higher dFdC:dFdU ratio and an increased amount of dFdCTP (active drug form) in tumors (Figure 7*A* and *B*). Thus, in addition to increased Gem delivery, ProAgio also increased the active drug form of Gem (dFdC) and decreased the inactive derivative (dFdU). We therefore asked how ProAgio prevented the conversion of Gem to its inactive metabolite. One mechanism by which PDAC becomes resistant to Gem is the conversion of Gem to dFdU by up-regulation of Cda.[31] Therefore, we histologically examined the enzyme Cda in tumors of ProAgio-treated mice. Cda is expressed primarily in the carcinoma cells. ProAgio and the combination decreased Cda expression in GEM-KPC and OrKPC tumors (Figure 7*C* and *D*). Immunoblot of tumor extracts confirmed the decrease in Cda in GEM-KPC tumors upon ProAgio treatment (Figure 7*E*). Gem is a prodrug form of dFdCTP. It needs to be converted to Gemcitabine monophosphate by an enzyme named deoxycytidine kinase (Dck). Pyrimidine kinase Thymidine kinase (Tdk) also is capable of increasing dFdCTP from Gem.[30] Thus, we examined whether an increase in dFdCTP under ProAgio treatment was owing to an increase in Dck and/or Tdk. Clearly, ProAgio did not alter Dck or Tdk in the tumor (Figure 7*F*–*I*). ProAgio also did not change the expression of multidrug resistance–associated protein 1 (ABCC1) (Figure 7*J*), another important player involved in cancer cell resistance to Gem.[31] It is known that IGF1 signaling plays an important regulatory role in Cda expression.[32,33] Examination of IGF1R phosphorylation and Cda levels in PDAC patient tissue samples showed a close correlation (Figure 8*A* and *B*), suggesting a possible role of IGF1R in regulating Cda in pancreatic cancer. The addition of IGF1 to the culture of KPC 961 cells up-regulated Cda expression in the cells (Figure 8*C*), verifying the role of IGF1 in up-regulation of Cda in this PDAC cell line. IGF1 is a common growth hormone, produced mainly by the liver in a healthy individual.[34] In cancerous tissue, CAFs are the main cells that secrete IGF1.[35–37] Furthermore, high insulin levels in pancreas may up-regulate IGF1 expression and activate Insulin-like growth factor 1 receptor (IGF1R signaling in PDAC tumor.[38] Because ProAgio depletes CAPaSC, we questioned whether ProAgio reduced IGF1 in PDAC, and thus consequentially suppressed Cda expression. We first examined the secretion of IGF1 by quiescent PaSC vs activated PaSC, and pancreatic cancer cells vs activated PaSC. Clearly, activated PaSC secrete higher levels of IGF1 than quiescent PaSC (Figure 8*D*). We also found that activated PaSC secrete higher levels of IGF1 than pancreatic cancer cells (Figure 8*E*). Furthermore, xenograft tumors of Panc1 co-implanted with PaSC secrete higher levels

Figure 2. (***See previous page***). **ProAgio depletes CAPaSC by targeting integrin $\alpha_V\beta_3$ and resorbs tumor collagen.** (*A* and *B*) Mean tumor volume of (*A*) subcutaneous xenograft of Panc1 with (*solid lines*) or without (*dotted lines*) co-implantation of PaSC and mean tumor weight (*B*) of Panc1 subcutaneous xenograft with or without co-implantation of PaSC upon treatment with vehicle (*black lines* in panel *A*, *grey dots* in panel *B*) or 10 mg/kg ProAgio (12 daily doses, *red lines* in panel *A*, *red dots* in panel *B*) (n = 6). (*C* and *E*) Representative images of immunofluorescence staining of α-SMA (red) (*C*) and Masson trichrome (blue) staining for collagen (*E*). (*D* and *F*) Quantitative analyses of immunofluorescence staining of α-SMA (*D*) and Masson trichrome (*F*) staining in tumor sections of Panc1 xenograft (with or without PaSC co-implantation) mice treated with vehicle or 10 mg/kg ProAgio. (*G* and *I*) Representative images of immunofluorescence staining of Ki67 (*G*, red) and CD31 (*I*, red). (*H* and *J*) Quantitative analyses of immunofluorescence staining of Ki67 (*H*) and quantification of mean vessel density, branch points, and vessel length based on CD31 staining (*J*) in tumor sections of Panc1 xenograft (with or without PaSC co-implantation) mice treated with vehicle or ProAgio. Quantification of Ki67 staining is presented as the percentage of $Ki67^+$ nuclei per view field (upper 3 panels, with PaSC co-implantation; bottom 3 panels, without PaSC co-implantation). (*C*, *G*, and *I*) Nuclei were stained with 4′,6-diamidino-2-phenylindole (DAPI) (blue). (*A* and *B*) Error bars represent means ± SEM. $^*P < .05$, $^{**}P < .01$, $^{***}P < .001$, $^{****}P < .0001$. n.s., denotes not significant.

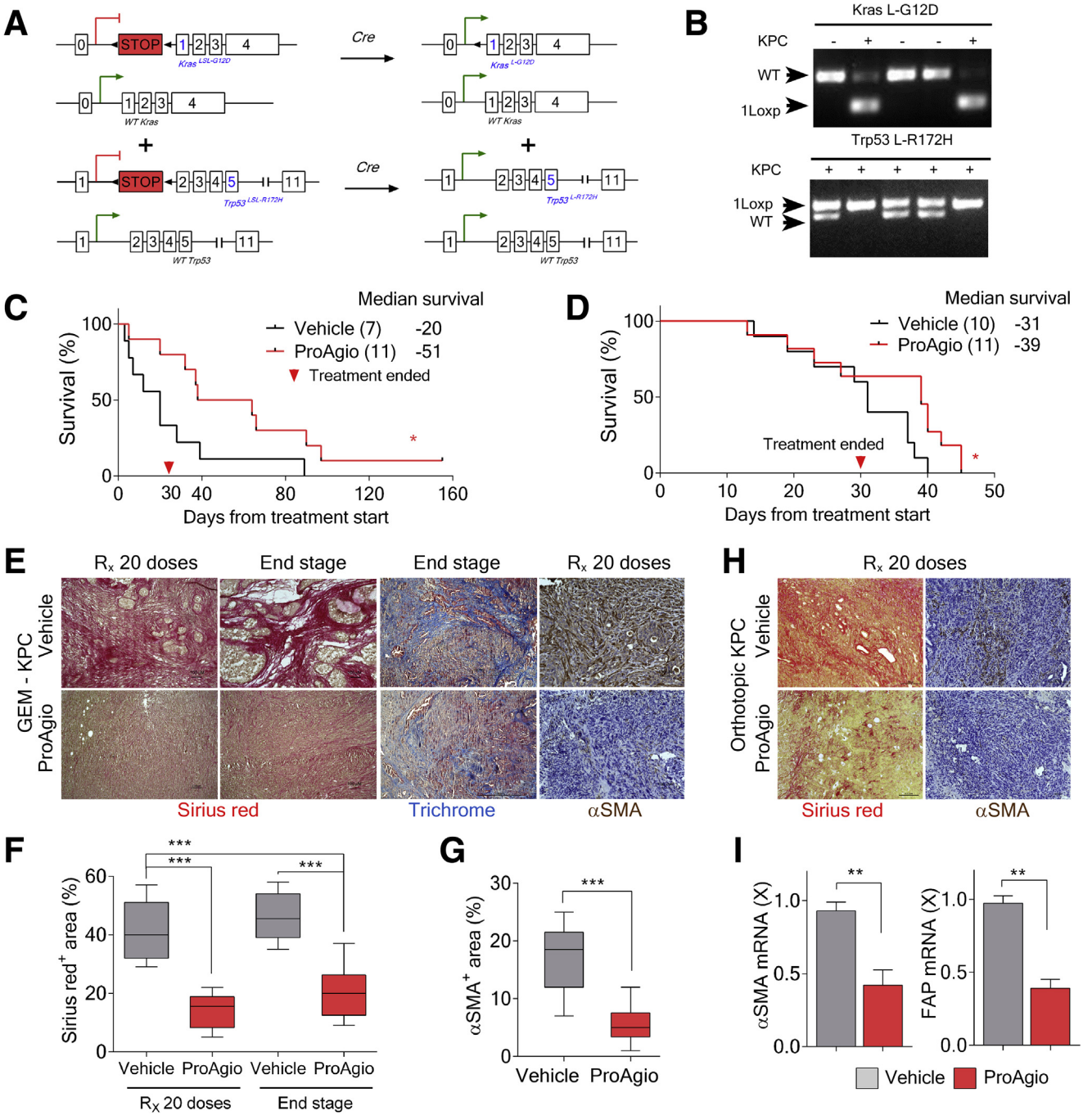

of IGF1 than the tumor without co-implantation (Figure 8*F*). We then examined the IGF1 levels in tumors of ProAgio and the combination treated GEM-KPC mice. Evidently, ProAgio and the combination led to a reduced IGF1 in GEM-KPC tumors (Figure 8*G* and *H*). In addition, the effect of ProAgio on IGF1 secretion was significantly higher in co-implanted tumors than without co-implantation in the Panc1 xenograft mouse model (Figure 8*F*). Our results support that ProAgio mediates reduced IGF1 levels in the tumor by CAPaSC depletion. ProAgio also led to a reduction in IGF1R phosphorylation in the tumors (Figure 8*I* and *J*). Consistently, in the presence of IGF1, KPC 961 cells were less susceptible to apoptosis induction by Gem (Figure 8*K*), and knockdown of Cda conferred KPC 961 cells more sensitive to apoptosis induction by Gem (Figure 8*L* and *M*).

Depletion of CAPaSC by ProAgio Decreases Hypoxia in PDAC Tumor

ProAgio and ProAgio plus Gem offered a very important advantage in PDAC treatment because a substantial decrease in metastasis was observed in GEM-KPC mice

(Figure 9*A*–*C*). A reduction in metastasis potentially has a critical impact on PDAC patient survival. Because ProAgio did not affect the pancreatic cancer cells, we wondered how ProAgio reduced PDAC metastasis. ProAgio reduced dense collagen bundles in the tumor, which disrupted the superhighway for PDAC cancer cell migration, and thus metastasis. In addition, ProAgio opened the collapsed blood vessels in PDAC tumor (Figure 4*A*–*E*), which would decrease hypoxia in tumor. Indeed, ProAgio decreased Hypoxia-inducible factor 1-alpha levels in the treated tumors (Figure 9*D* and *E*). Hypoxia is known to up-regulate and activate IGF1R.[39] ProAgio decreased IGF1 owing to depletion of CAPaSC in the tumor. ProAgio also decreased hypoxia. We therefore believe that the effect of ProAgio on IGF1R signaling, in addition to reducing cancer cell apoptosis resistance,[40] also might play a role in PDAC metastasis. Cell migration assay showed that IGF1 stimulated cell migration under hypoxia condition, while IGF1 had limited effects on cell migration under normoxic conditions. The effect of IGF1 on cell migration was dose-dependent because IGF1 had no effect on migration at a concentration as low as 1 ng/mL (Figure 9*F*–*I*).

Effects of Specific Targeting of CAPaSC by ProAgio

Despite the known protumorigenic properties of CAF, recent studies have suggested that depletion of fibrotic stroma has the potential to accelerate the disease and lead to cancer progression.[8–10] To assess how CAPaSC depletion by ProAgio affects the differentiation and aggressiveness of PDAC tumors, we analyzed tumor tissue from GEM-KPC mice at the end of the survival experiment. In concert with longer survival, tumors from ProAgio-treated GEM-KPC mice were more differentiated and had a decreased pathologic disease progression compared with vehicle-treated mice (Figure 10*A* and *B*). We analyzed the proliferation marker Ki67 in vehicle- and ProAgio-treated mice and found that ProAgio-treated mice had decreased cell proliferation (Figure 10*C* and *D*). ProAgio also significantly decreased tumor metastases to the liver (Figure 9*A*–*C*). We asked why targeting fibrotic stroma by ProAgio did not result in more poorly differentiated and aggressive tumor as observed by other strategies that target fibrotic stroma.[8–10] The important difference is that ProAgio induces apoptosis via targeting integrin $\alpha_v\beta_3$. In PDAC, only CAPaSC are integrin $\alpha_v\beta_3$ positive, while inactivated PaSC are $\alpha_v\beta_3$ negative. ProAgio only depletes the CAPaSC, leaving the normal or quiescent PaSC intact. To verify this unique targeting property, we examined the status and levels of PaSC by retinol staining (retinol stains inactivated PaSC) in the treated GEM-KPC tumors. Clearly, there was almost no inactivated PaSC in vehicle-treated tumors. However, the inactivated PaSC levels were higher in tumors of ProAgio plus Gem–treated animals (Figure 10*E* and *F*). Furthermore, we stained the tumor sections with adipophilin, a marker for quiescent PaSC,[41] and cleaved Poly (ADP-ribose) polymerase (PARP), an apoptosis marker. Consistent with retinol staining, there was less adipophilin stain in the sections of vehicle-treated animals. ProAgio led to an approximately 2-fold, and ProAgio plus Gem led to more than a 6-fold, increase in adipophilin staining compared with those of the vehicle-treated group (Figure 10*G* and *H*). There was almost no adipophilin and cleaved PARP co-stain in any case. Thus, both in vitro and in vivo studies have suggested that ProAgio specifically induces CAPaSC apoptosis. We do not fully understand the mechanism by which ProAgio and ProAgio plus Gem lead to an increase in inactivated/quiescent PaSC in tumor. It is possible that the treatments, especially the combination, removed cancer cells. Thus, PaSC activation by cancer cells is reduced. The explanation is consistent with the fact that the increase in inactivated PaSC in the ProAgio plus Gem group is higher than in the ProAgio alone group.

Discussion

We show here that targeting integrin $\alpha_v\beta_3$ by ProAgio specifically induces apoptosis of CAPaSC. CAPaSC are the major source of collagen secretion in PDAC tumor. On the other hand, there are numerous sources (cancer cells, immune cells) for Matrix metalloproteinases secretion, which can digest collagen. Thus, ProAgio enables reduction of stromal collagen in the tumor. Reduction of collagen consequently opened the collapsed tumor vessels. Removal of a physical block by depletion of dense collagen and opening of collapsed vessels resulted in increased delivery

Figure 3. (***See previous page***). **ProAgio depletes CAPaSC by targeting integrin $\alpha_v\beta_3$ and resorbs tumor collagen.** (*A*) Endogenous alleles of *KrasG12D* and *Trp53R172H* are conditionally activated in the pancreata of *LSL-KrasG12D/+*; *LSL-Trp53R172H/+*; *Pdx-1-Cre* (triple mutant) mice. (*B*) Specific polymerase chain reaction analysis of genomic DNA of generated GEM-KPC mice. (*C* and *D*) Kaplan–Meier survival analysis of GEM-KPC (median survival: vehicle, 20 days; ProAgio, 51 days) (*A*), and OrKPC (*B*) mice treated with vehicle or 10 mg/kg ProAgio (median survival: vehicle, 31 days; ProAgio, 39 days) (10 daily doses + 10 alternate day doses). Treatment was started after 13 weeks of age in GEM-KPC mice in panel *C*, or 30 days after tumor inoculation in panel *D*. The numbers in parentheses indicate the group size. (*E*) Representative images of Sirius red (red) and Masson trichrome (blue) staining and IHC staining of α-SMA of tumor sections from GEM-KPC mice treated with vehicle or 10 mg/kg ProAgio at different time points (R_x 20, at end of 20 doses; End stage, end of survival experiments). (*F* and *G*) Quantitative analyses of Sirius red staining (presented as Sirius red$^+$ area %) (*F*) and αSMA$^+$ staining area % (*G*) in tumor sections of vehicle or ProAgio-treated (10 mg/kg) GEM-KPC mice. A higher staining of Sirius red was observed in vehicle-treated tumors on day 80 (R_x 20 doses) than ProAgio-treated tumors on day 110 (end stage) in GEM-KPC mice ($P < .001$; n = 7–9). (*H*) Representative images of Sirius red (Sirius red) and IHC staining of α-SMA in tumor sections of vehicle or ProAgio-treated (10 mg/kg) OrKPC mice at the end of 20 doses (R_x 20 doses). (*I*) mRNA levels of α-SMA (*left panel*) and FAP (*right panel*) in the tumor tissue lysates of GEM-KPC mice treated with vehicle or ProAgio (n = 4) were analyzed by quantitative reverse-transcription polymerase chain reaction. The mRNA levels in the tumor extracts were normalized to mRNA level of β-actin. (*G*) Error bars represent means ± SEM. **P* < .05, ***P* < .01, ****P* < .001, *****P* < .0001. n.s., denotes not significant; WT, wild-type.

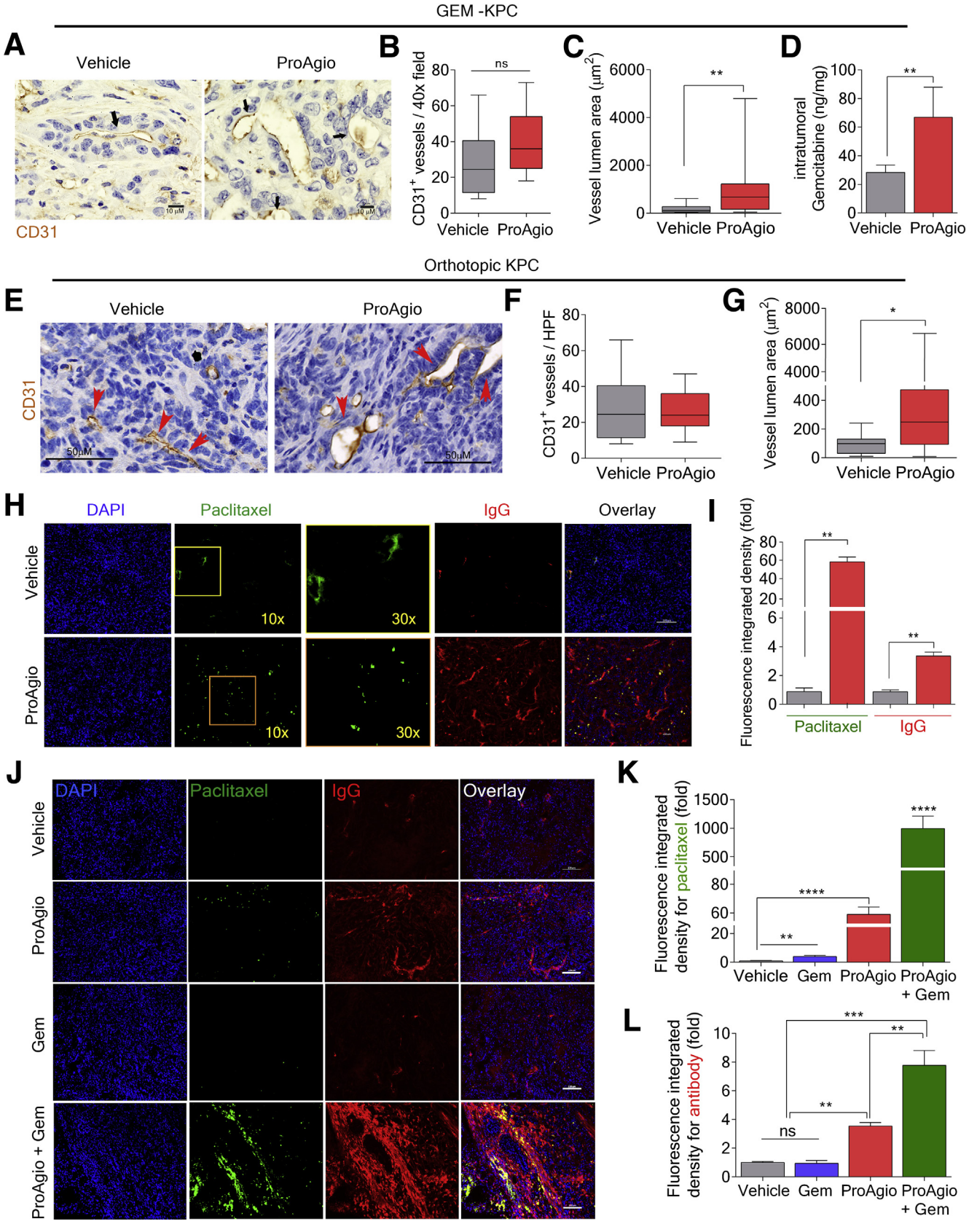
GEM -KPC
A
Vehicle
ProAgio
CD31
B
CD31+ vessels / 40x field
ns
Vehicle ProAgio
C
Vessel lumen area (μm2)
**
Vehicle ProAgio
D
intratumoral Gemcitabine (ng/mg)
**
Vehicle ProAgio
Orthotopic KPC
E
Vehicle
ProAgio
CD31
50μM
F
CD31+ vessels / HPF
Vehicle ProAgio
G
Vessel lumen area (μm2)
*
Vehicle ProAgio
H
DAPI
Paclitaxel
IgG
Overlay
Vehicle
ProAgio
10x
30x
I
Fluorescence integrated density (fold)
**
Paclitaxel
IgG
J
DAPI
Paclitaxel
IgG
Overlay
Vehicle
ProAgio
Gem
ProAgio + Gem
K
Fluorescence integrated density for paclitaxel (fold)
****
**
Vehicle Gem ProAgio ProAgio + Gem
L
Fluorescence integrated density for antibody (fold)
***
**
**
ns
Vehicle Gem ProAgio ProAgio + Gem

of drug molecules into the tumor. Induction of apoptosis of CAPaSC by ProAgio also remarkably reduced IGF1, and possible other growth factors and cytokines, which is produced mainly by CAF in cancerous tissue, and consequently resulted in a decrease and inactivation of IGF1R in cancer cells. A decrease and inactivation of IGF1R suppressed Cda expression, which stabilized Gem in cancer cells equivalent to an increase in active Gem concentration in cancer cells. Moreover, opening the collapsed blood vessels reduced hypoxia. A reduction in hypoxia in conjunction with decreased IGF1 and inactivation of IGF1R decreased cancer cell migration, thereby decreasing cancer metastasis. Thus, it is clear that ProAgio enacts multiple effects on PDAC by specifically acting on CAPaSC and angiogenic endothelial cells (Figure 10*I*).

It generally is believed that dense fibrotic stroma is a major obstacle for successful treatment of PDAC. CAF supports cancer cell growth, survival, resistance to apoptosis, and metastasis. Thus, it is speculated that depletion of fibrotic stroma would be therapeutically advantageous in PDAC. However, recent studies of Shh and α-SMA gene deletion in PDAC GEM models suggest that some fibrotic stroma in PDAC may constitute a barrier that prevents metastatic spread of the tumor.[8–10] Depletion of fibrotic stroma results in increased metastasis and shorter survival in preclinical models and some early phase clinical studies.[8,9,11] These studies caused a very important controversy, "target or not-target fibrotic stroma in cancer therapies, particularly in treatment of PDAC?"[12] It should be noted that Shh or α-SMA gene deletion leads to global deletion of fibroblasts, resulting in downstream effects in excess of what would be expected from a tumor-targeted therapeutic. Pharmacologic inhibition of Shh signaling also may impose effects far beyond fibroblasts. Importantly, unlike globally targeting fibroblasts, specifically acting on CAF by ProAgio may confer an advantage in cancer therapy. Indeed, ProAgio treatment did not lead to more aggressive cancer with increased metastasis and did not increase angiogenesis in the tumor as observed with Shh or α-SMA gene deletion or Shh inhibition. A recent large-scale patient tumor study showed that the percentage of stromal cells determines the phenotypic nature of PDAC, wherein an increase in stromal cells leads to high proliferative and high migratory phenotype. The effectiveness of ProAgio in PDAC treatment provides a good explanation for the observation because ProAgio specifically depletes CAPaSC, leading to a decrease in PDAC cancer cell proliferation and migration.[43]

One main advantage of targeting integrin $\alpha_v\beta_3$ by ProAgio is the decrease in PDAC metastasis upon ProAgio treatment (Figure 9*A–C*). Our experiments showed that ProAgio affects the metastasis of tumor cells by the following mechanisms: (1) ProAgio depletes CAPaSC, which encourages tumor cell metastasis; (2) ProAgio decreases collagen, which provides a superhighway for tumor cell migration–metastasis; (3) ProAgio opens collapsed PDAC blood vessels, which decreases tumor hypoxia, and a decrease in tumor hypoxia reduces tumor cell metastasis; and (4) IGF1 promotes the migration of KPC cells, particularly under hypoxia conditions. ProAgio reduces IGF1 levels in the tumor by depleting CAPaSC and therefore reduces metastasis.

Enzymatic inactivation of gemcitabine is the main reason leading to cancer resistance to this anticancer drug. Intriguingly, ProAgio decreases IGF1 by depleting CAPaSC, which consequently suppresses Cda expression in cancer cells. Our data clearly show that activated PaSC have significantly higher IGF1 secretion compared with the quiescent PaSC and pancreatic cancer cells (Figure 8*D* and *E*). IGF1 secretion is higher in Panc1 tumors co-implanted with PaSC compared with tumor without co-implantation (Figure 8*F*). Furthermore, ProAgio had greater effects on IGF1 secretion in Panc1 tumors with PaSC co-implantation

Figure 4. (***See previous page***). **ProAgio opens compressed tumor vessels and increases drug delivery.** (*A*) Representative images of IHC staining of CD31 from GEM-KPC mice tumor sections treated with vehicle or 10 mg/kg ProAgio. *Arrows* indicate example vessels. (*B* and *C*) Quantification of CD31-positive vessel density (*B*), and mean vessel lumen area (*C*) in tumor sections of vehicle or ProAgio-treated GEM-KPC mice. (*D*) Intratumoral Gem levels measured in extracts of tumors of vehicle and ProAgio-treated (after 8 daily doses) GEM-KPC mice 2 hours after intravenous dose of Gem (n = 6). Gem levels were presented as nanogram of Gem per milligram of tumor tissue. (*E*) Representative images of IHC staining of CD31 in tumor sections of vehicle or ProAgio-treated OrKPC mice. *Arrows* indicate the tumor vessels. (*F* and *G*) Quantitative analyses of CD31 vessel stain density (*F*) and vessel lumen area (*G*) in tumor sections of vehicle or ProAgio-treated OrKPC mice. (*H* and *I*) Representative fluorescence images of Alexa Fluor 555–conjugated IgG, approximately 160 kilodalton (red) and Alexa Fluor 488–conjugated paclitaxel, approximately 1 kilodalton (green; *left panel*, 10×; *right panel*, 30×) (*H*) and quantification of fluorescence signals from paclitaxel and IgG (*I*) in tumor sections of vehicle or ProAgio-treated OrKPC mice using ImageJ. (*J–L*) Representative fluorescence images of Alexa Fluor 555–conjugated IgG, approximately 160 kilodalton (red) and Alexa Fluor 488–conjugated paclitaxel, approximately 1 kilodalton (green) (*J*) and quantification of fluorescence signals (*K* and *L*) in tumor sections of OrKPC mice treated with the indicated agents. Quantification is presented as fold change of the fluorescence integrated density (fold) by comparing it with the mean value of the vehicle treatment group as 1. Image analysis was performed by thresholding for positive staining and normalizing to total tissue area. (*H* and *I*) Fluorescence probe conjugated IgG and paclitaxel were injected intravenously after 8 daily doses of 10 mg/kg ProAgio treatment. (*J–L*) Fluorescence probe–conjugated IgG and paclitaxel were injected intravenously after 8 daily doses of ProAgio (ProAgio), 3 doses of Gem (Gem), or 8 doses of ProAgio plus 3 doses of Gem (ProAgio + Gem) treatments. Tumors were harvested and processed 40 minutes after the intravenous injection (analyses: n = 5 mice per treatment group, n = 7–8 images per mouse). Nuclei were stained with 4′,6-diamidino-2-phenylindole (DAPI) (blue), and yellow indicates colocalization. (*D*, *I*, *K*, and *L*) Error bars represent means ± SEM. **P* < .05, ***P* < .01, ****P* < .001, *****P* < .0001. n.s., denotes not significant.

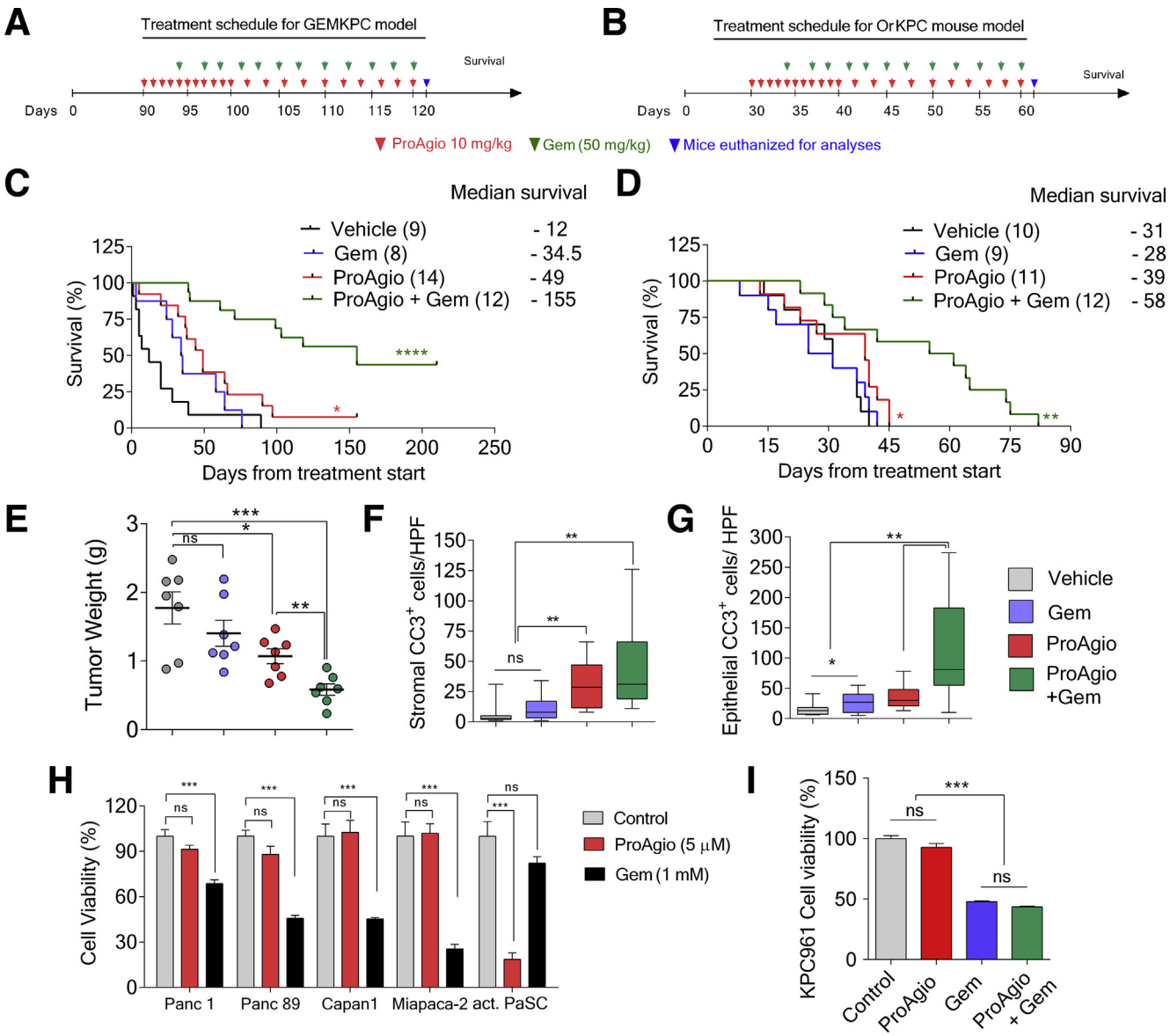

Figure 5. Depletion of CAPaSC by ProAgio enhances the effectiveness of gemcitabine. (*A* and *B*) The 10 mg/kg ProAgio and 50 mg/kg Gem treatment regimen of GEM-KPC (*A*) and OrKPC (*B*) mice. (*C* and *D*) Kaplan–Meier survival analyses of GEM-KPC (median survival: vehicle, 12 days; Gem, 34.5 days; ProAgio, 49 days; ProAgio + Gem, 155 days) (*C*), and OrKPC (median survival: vehicle, 31 days; Gem, 28 days; ProAgio, 39 days; ProAgio + Gem, 58 days) (*D*) mice upon indicated treatments. The numbers in the parentheses are the group size. (*E*) Mean tumor weight of OrKPC mice (n = 7) treated with the indicated agents at the end of treatment (mice were killed at the end of the treatment and tumors were resected and weighed). (*F* and *G*) Quantification of IHC staining of cleaved caspase 3 in stromal areas (stromal $CC3^+$ cells/high-power field [HPF], cleaved caspase 3–positive cells per view field) (*F*) and adenocarcinoma area (epithelial $CC3^+$ cells/HPF) (*G*) in tumor sections from GEM-KPC mice upon indicated treatments. (*H*) Cell viability of indicated cells upon treatment with ProAgio (5 μmol/L) and Gem (1 mmol/L) was analyzed by MTT assay. (*I*) The cell viability of KPC 961 cells treated with ProAgio, Gem, and ProAgio plus Gem combination was analyzed by MTT assay. (*H* and *I*) The viability of vehicle-treated cells (control) was defined as 100%. (*E*, *H*, and *I*) Error bars represent means ± SEM. MTT, 3-(4,5-Dimethylthiazol-2-yl)-2,5-diphenyltetrazolium bromide.

(Figure 8*F*). The results suggest that ProAgio mediates reduced IGF1 levels by CAPaSC depletion. It recently was shown that CAPaSC also traps Gem in the cancer stroma.[43] Depletion of CAPaSC by ProAgio would release the trapped Gem and increase available Gem to cancer cells. Because Gem has been approved for the treatment of multiple different cancer types,[29] it will be interesting to test whether the same mechanism will be true for the Gem treatment resistance in other cancers.

Materials and Methods

Primary Human Pancreatic Stellate Cells and Activation

Primary human pancreatic stellate cells were purchased from Cell Biologics (Chicago, IL). The cells were cultured according to the manufacturer's instructions. PaSC were activated by culturing them for 48 hours in the presence of 5 ng/mL transforming growth factor-β.

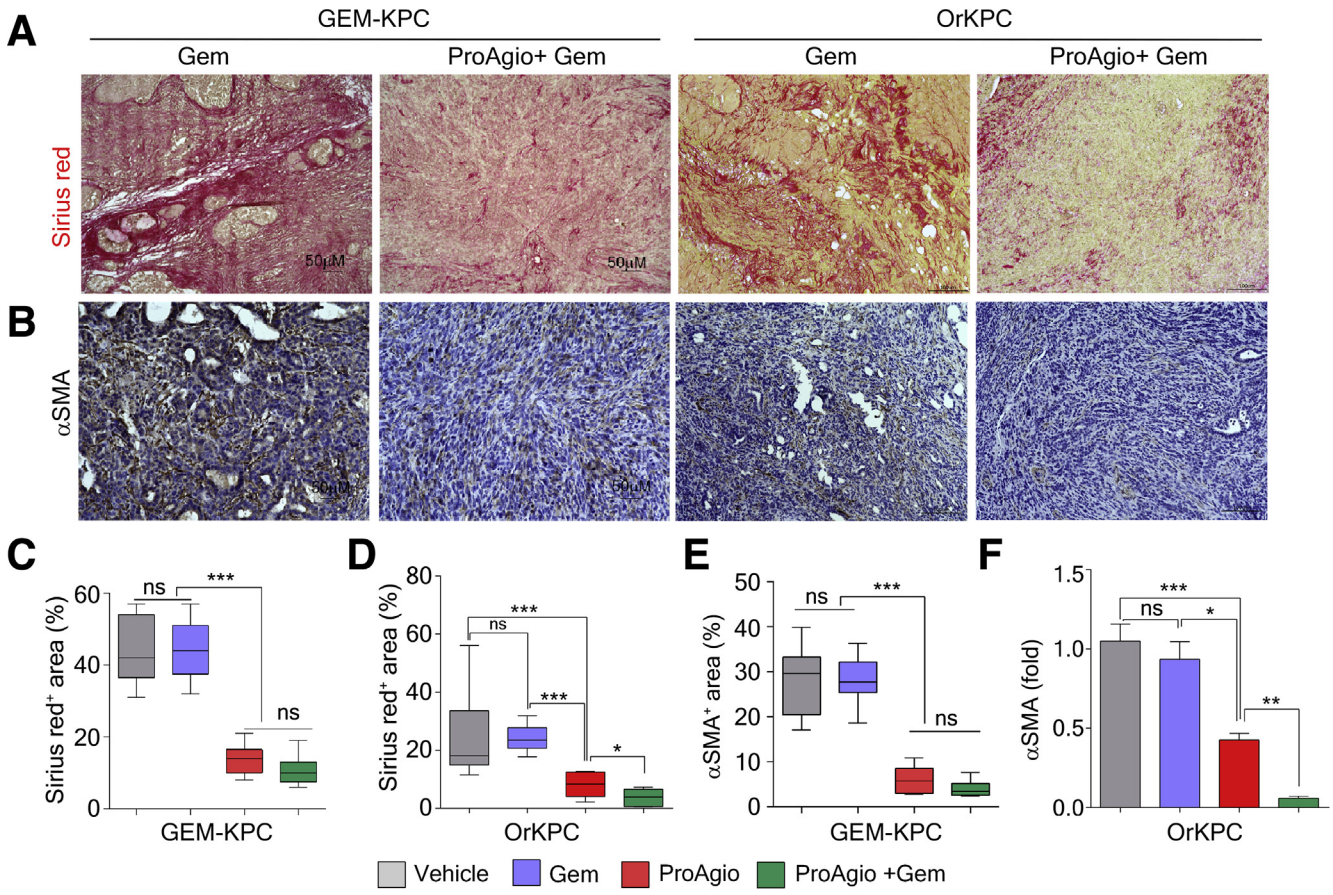

Figure 6. ProAgio plus Gem further reduces intratumoral collagen and CAPaSC. (*A* and *B*) Representative images of Sirius red staining (*A*) and IHC staining of α-SMA (*B*) in tumor sections from GEM-KPC and OrKPC mice treated with the indicated agents. (*C–F*) Quantitative analyses of Sirius red stain area (Sirius red$^+$ area %) (*C* and *D*) and IHC α-SMA stain area (α-SMA$^+$ area %) (*E* and *F*) in sections of tumors from GEM-KPC and OrKPC mice treated by the indicated agents. (*F*) Error bars represent means ± SEM. *$P < .05$, **$P < .01$, ***$P < .001$, ****$P < .0001$. n.s., not significant.

Panc1 Xenograft, GEM-KPC, and OrKPC Mice Generation and Treatments, and Patient Tissue Sample Screening

All animal experiments were performed under approval of the Institutional Animal Care and Use Committee of Georgia State University.

Panc1 xenograft. Panc1 (1×10^6) cells with/without (1:1 ratio) activated human PaSC (1×10^6) were implanted into the right flank of nude mice. Tumor growth was measured using a caliper ruler.

GEM-KPC. LSL-Kras$^{G12D/+}$; LSL-Trp53$^{R172H/+}$; Pdx-1-Cre mice were purchased from Jackson Laboratory (Bar Harbor, ME). GEM-KPC mice were generated by crossing LSL-Kras$^{G12D/+}$ with LSL-Trp53$^{R172H/+}$, and subsequently crossing with Pdx-1-Cre.

OrKPC. First, C57BL/6J mice were anesthetized. The pancreas was exposed through an abdominal incision. A single-cell suspension of 0.5×10^5 KPC 961 cells in 50 μL Hank's balanced salt solution was injected directly into the pancreas using a 30G needle. After injection, the mice without leakage during injection were included in the experiments. After inoculation, the pancreas was returned carefully to the peritoneal cavity and the abdomen was closed. After tumor implantation, all mice were returned to their cages and monitored daily. GEM-KPC mice treatments were started at 14 weeks of age. For OrKPC mice, treatments were started approximately 30 days after tumor inoculation. Mice were enrolled in treatment groups randomly and palpated twice a week for evidence of tumor after group division. A portion of each group of mice were examined by ultrasound imaging to confirm the evidence of tumor presence. At the end of the treatments, animals either were killed for analyses or maintained in the cages for survival assessment. Organs, tumor tissues, and blood samples were collected at the end of the experiments for subsequent analyses. For all treatments, the vehicle administered was ProAgio formulation buffer in which ProAgio is dissolved, the ProAgio dose was 10 mg/kg, and Gem was 50 mg/kg via intraperitoneal injection. A 10-mg/kg dose was chosen based on our previous dose response in the in vivo analyses.[16] The treatment schedule is specified in figures or legends. Statistical analyses were performed in comparison with the control group.

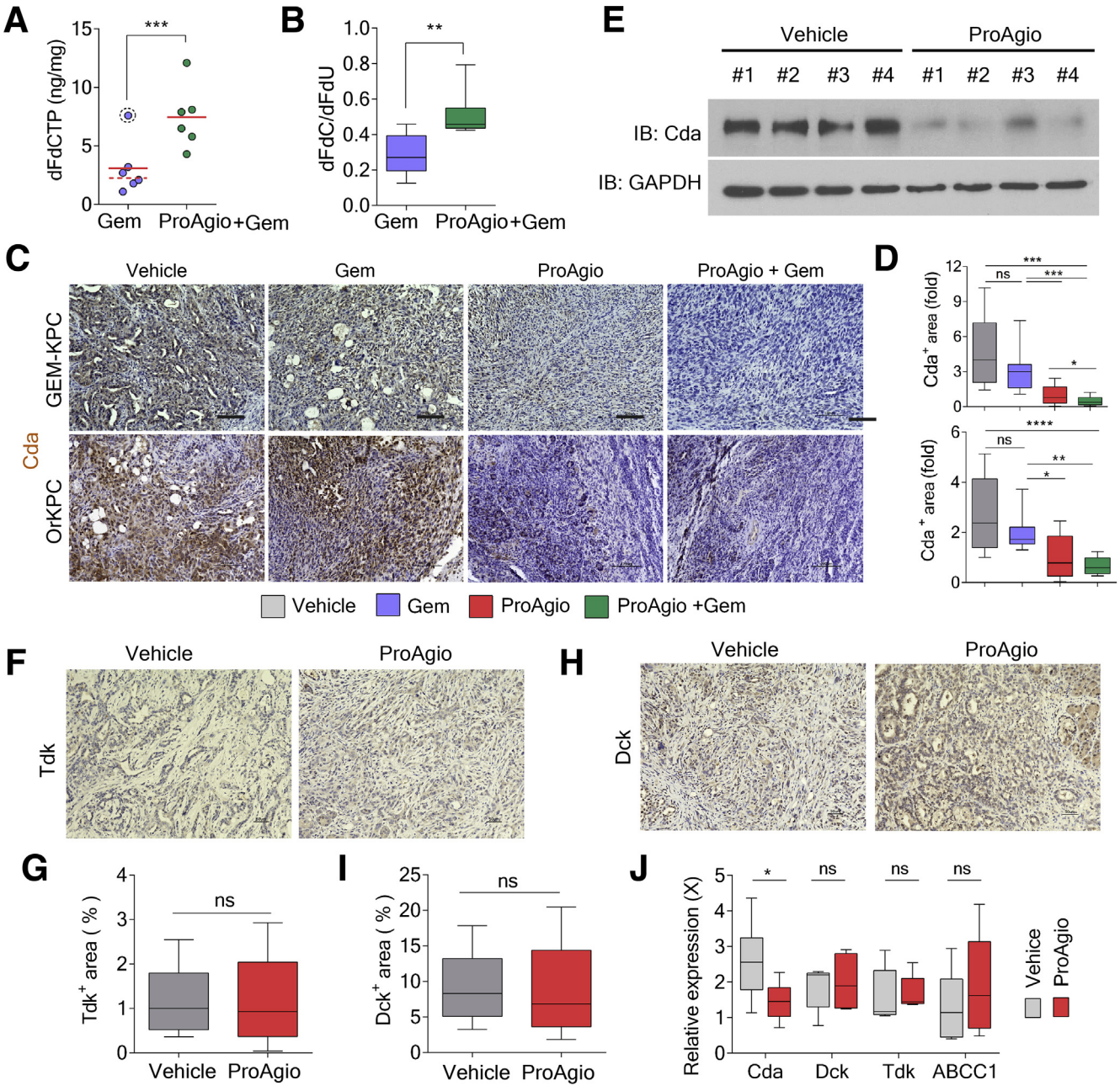

Figure 7. Depletion of CAPaSC by ProAgio alters Gem metabolism and reduces cancer cell resistance to Gem. (*A* and *B*) Intratumoral levels of dFdCTP (*A*) and the dFdC:dFdU ratio (*B*) in tumor tissues of GEM-KPC mice treated with the indicated agents measured by high-performance liquid chromatography/mass spectrometry. The concentration of dFdCTP, dFdC, and dFdU in tumor tissues was analyzed 2 hours after the last dose of Gem (n = 6). (*C* and *D*) Representative images of IHC staining of Cda (*C*) and quantitation of IHC staining of Cda (*D*) (Cda^+ area [fold], fold change by comparison with the mean value of the ProAgio group as 1) in tumor sections of GEM-KPC and OrKPC mice treated with the indicated agents. (*E*) The levels of Cda (IB:Cda) in tumor extracts of vehicle or ProAgio-treated GEM-KPC mice were analyzed by immunoblot. Immunoblot of glyceraldehyde-3-phosphate dehydrogenase (GAPDH) (IB:GAPDH) is a loading control. (*F* and *H*) Representative images of IHC staining of Tdk (*F*) and Dck (*H*), and (*G* and *I*) quantitative analyses of Tdk-positive stain area (*G*) and Dck-positive stain area (*I*) in tumor sections of ProAgio-treated GEM-KPC mice. (*J*) The mRNA levels of Cda, Dck, Tdk, and ABCC1 genes in the tumor extracts of the indicated treatment cohorts (n = 6) were analyzed by quantitative reverse-transcription polymerase chain reaction. The mRNA levels in the tumor extracts were normalized to the mRNA level of GAPDH. (*A*) Error bars represent means ± SEM. IB, immunoblot.

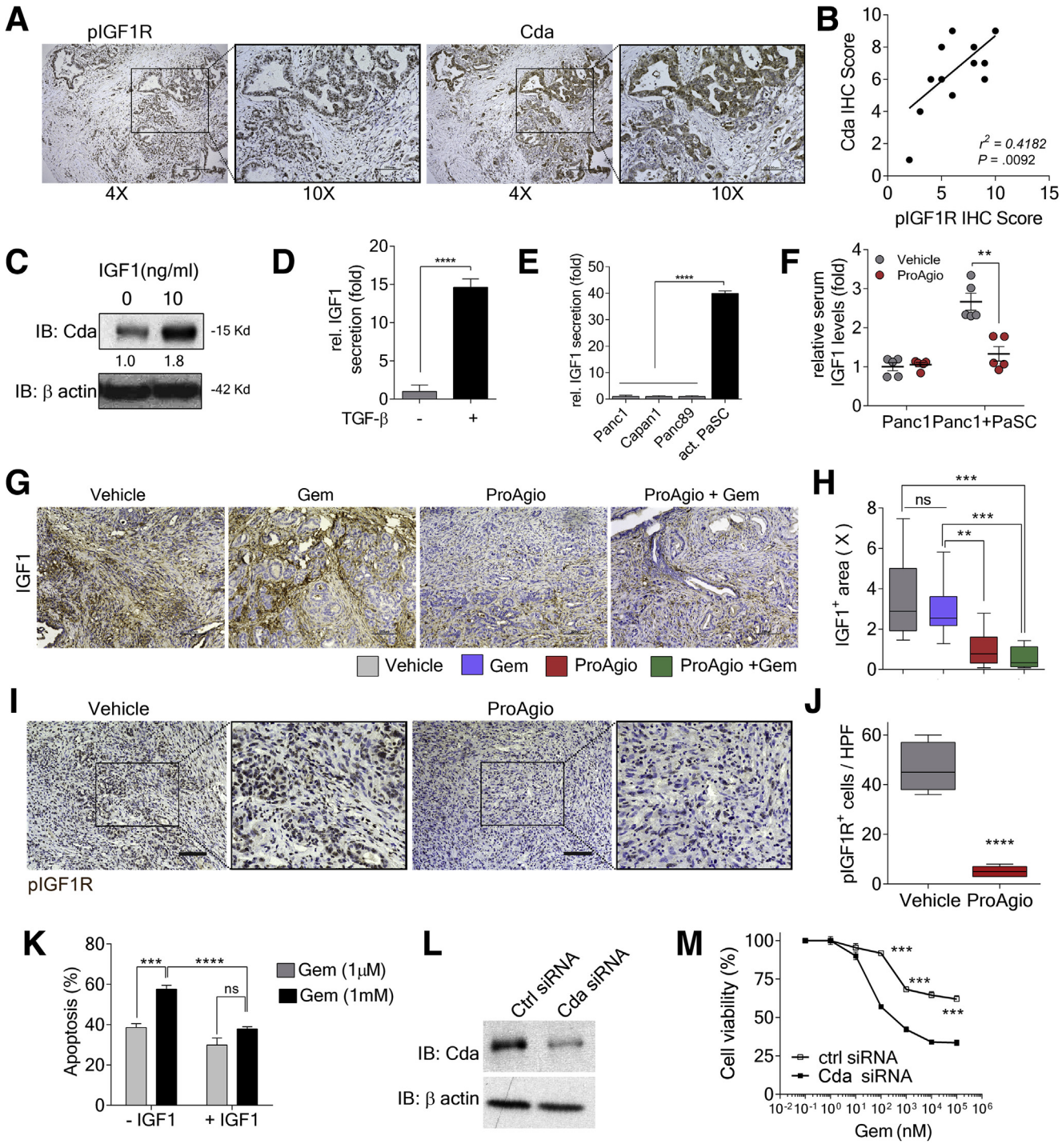

Patient tissue analyses were performed in accordance with the National Institutes of Health guidelines. All tissue samples are de-identified, which falls under Institutional Review Board exemption 4. Tissue samples were sectioned and analyzed by immunohistochemical (IHC) staining. Samples were obtained either from commercial sources or the Emory-Winship Cancer Center patient tissue bank.

Tissue Section Staining

Sirius red, Masson trichrome, and Oil red O staining were performed using kits obtained from IHC WORLD (Woodstock, MD) by following the vendor's instructions.

IHC and immunofluorescence. The IHC and immunofluorescence staining procedures were similar to those of previous reports.[17] Images were captured at various

magnification lens apertures and indicated by scale bars in the images.

Quantitation of Sirius red, Masson trichrome, Oil red O, IHC, and immunofluorescence staining was performed using ImageJ software (National Institutes of Health, Bethesda, MD). Quantities are presented as the percentage of positive stain area in each view field or fold change by comparison with the control (vehicle) unless otherwise specified in the figures and legends. All quantitation results were means of 3 randomly selected view fields per section, 5 sections per animal, and 6–10 mice per experimental group, unless otherwise specified in the figures and legends.

Mean Vascular Density and Mean Vessel/Lumen Area

The mean vascular density was determined as the number of CD31-positive staining tumor samples per 40× field. For OrKPC and KPC GEM tumor samples, the mean vessel/lumen area was a measurement of CD31-positive stained areas using ImageJ software. Three view fields per section, 5 sections per tumor, were quantified as described in our previous report.[17]

Determination of dFdCTP, dFdU, and dFdC Concentrations in Tumors by High-Performance Liquid Chromatography/Mass Spectrometry

Tissues from treated mice were dissected rapidly and snap-frozen in liquid nitrogen. The specimens were ground in liquid nitrogen, suspended in 0.4 N perchloric acid, and sonicated in an ice bath. Precipitates were removed by centrifugation, the pellet was washed with perchloric acid, and the supernatants were combined. After neutralization with potassium hydroxide and removal of $KClO_4$ by centrifugation, a portion of the supernatant was analyzed for dFdCTP, dFdU, and dFdC in the samples by high-performance liquid chromatography, as described in previous studies. High-performance liquid chromatography analyses were performed using an Agilent Technologies (Santa Clara, CA) UHPLC system with a Zobax column. The mobile phase was a mixture of acetonitrile (A) and 0.1% formic acid in water (B) with a gradient elution. The flow rate was 0.6 mL/min. Mass spectrometric analysis was performed on a 6545QTOF mass spectrometer equipped with an electrospray ionization source in positive mode. During all the runs, the Quadrupole Time-of-Flight was calibrated by 2 reference masses (121.0508 and 922.0097 daltons) flowing at a continuous flow rate of 100 μL/min. Before analysis, the time of flight/mass spectrometry was calibrated using a reference solution consisting of masses (121.0508, 149.0233, 322.0481, 922.0097, 1221.9906, and 1521.9714 daltons) with a resolution greater than 10,000. For gemcitabine and dFdU, linearity was established in aqueous solution and saline. The method developed was sensitive and specific with no interference from the matrix at the retention of analytes or internal standard with an lower limit of quantitation of 7.81 nmol/L for both analytes. Phenacetin (500 ng/mL) was used as an internal standard. All samples were analyzed with calibration curve standards spanning a range of 7.81 to 1000 nmol/L. The amount of gemcitabine triphosphate was normalized to the adenosine triphosphate level determined in the same sample.

Statistical Calculations

Statistical analyses were performed using GraphPad Prism 6.0 software (Graphpad Holdings, LLC, La Jolla, CA). Kaplan–Meier survival curves were calculated using the survival time for each mouse from all treatment groups. Statistical analyses in the survival experiments were performed by log-rank (Mantel–Cox) test. All in vitro experiments were performed at least 5 times. For tumor burden analyses, image quantifications, and other analyses, statistical significance was assayed by unpaired Student *t* test. Box plots show ranges, medians, and quartiles.

Figure 8. (***See previous page***). **ProAgio decreases Cda in cancer cells by decreasing IGF1 signaling.** (*A*) Representative images of IHC staining of pIGF1R (*left panel*; 4× and 10× enlarged images) and Cda (right panel, 4× and 10× enlarged images) in tumor sections of PDAC patients (n = 40). (*B*) Correlation of pIGF1R protein expression with Cda protein expression. Regression analysis for expression of the pIGF1R (IHC) vs Cda (IHC) in tumor sections of PDAC patients (n = 12). (*C*) The levels of Cda (IB:Cda) in KPC 961 cells that were treated with IGF-1 (0 ng/mL and 10 ng/mL) were analyzed by immunoblot. (*D*) Levels of IGF1 secreted by inactivated PaSC (without transforming growth factor [TGF]-β, *grey bar*) or activated PaSC (with 5 ng/mL TGF-β, *black bar*). (*E*) Levels of IGF1 secreted by the indicated cells. (*F*) Levels of IGF1 in the serum of a subcutaneous xenograft mouse model of Panc1 or Panc1 co-implanted with activated human PaSC treated with vehicle or ProAgio (n = 5). IGF1 levels were analyzed by enzyme-linked immunosorbent assay. (*G* and *H*) Representative images of IHC staining of IGF1 (*G*) and quantitation of IHC staining of IGF1 (*H*) (IGF1$^+$ area [X], fold change by comparison with the mean value of the ProAgio group as 1) in tumor sections of GEM-KPC mice treated with the indicated agents. (*I* and *J*) Representative images of IHC staining of pIGF1R (*I*) and quantitation of pIGF1R-positive staining (*J*, pIGFR$^+$ cells/HPF, pIGFR-positive cells per view field) in tumor sections of vehicle or ProAgio-treated OrKPC mice. (*K*) Apoptosis of KPC 961 cells after treatment with Gem (1 μmol/L, *grey bar*, or 1 mmol/L, *black bar*) in the presence (+IGF1) or absence (-IGF1) of 10 ng/mL IGF1 was measured by an apoptosis kit. Cell apoptosis is presented as the percentage of apoptosis by defining the apoptosis of untreated cells as 0%. (*L*) The levels of Cda (IB:Cda) in KPC 961 cells after Cda knockdown (Cda small interfering RNA [siRNA]) compared with control (ctrl siRNA) were analyzed by immunoblot. (*M*) Cell viability of KPC 961 cells with (Cda siRNA) or without (ctrl siRNA) knockdown of Cda treated with the indicated concentrations of Gem was measured by MTT assay. (*C* and *L*) Immunoblot of β-actin (IB:β-actin) is a loading control. (*D*, *E*, *F*, *K*, and *M*) Error bars represent means ± SEM. MTT, 3-(4,5-Dimethylthiazol-2-yl)-2,5-diphenyltetrazolium bromide; pIGF1R, Phospho-IGF-I Receptor; X, times.

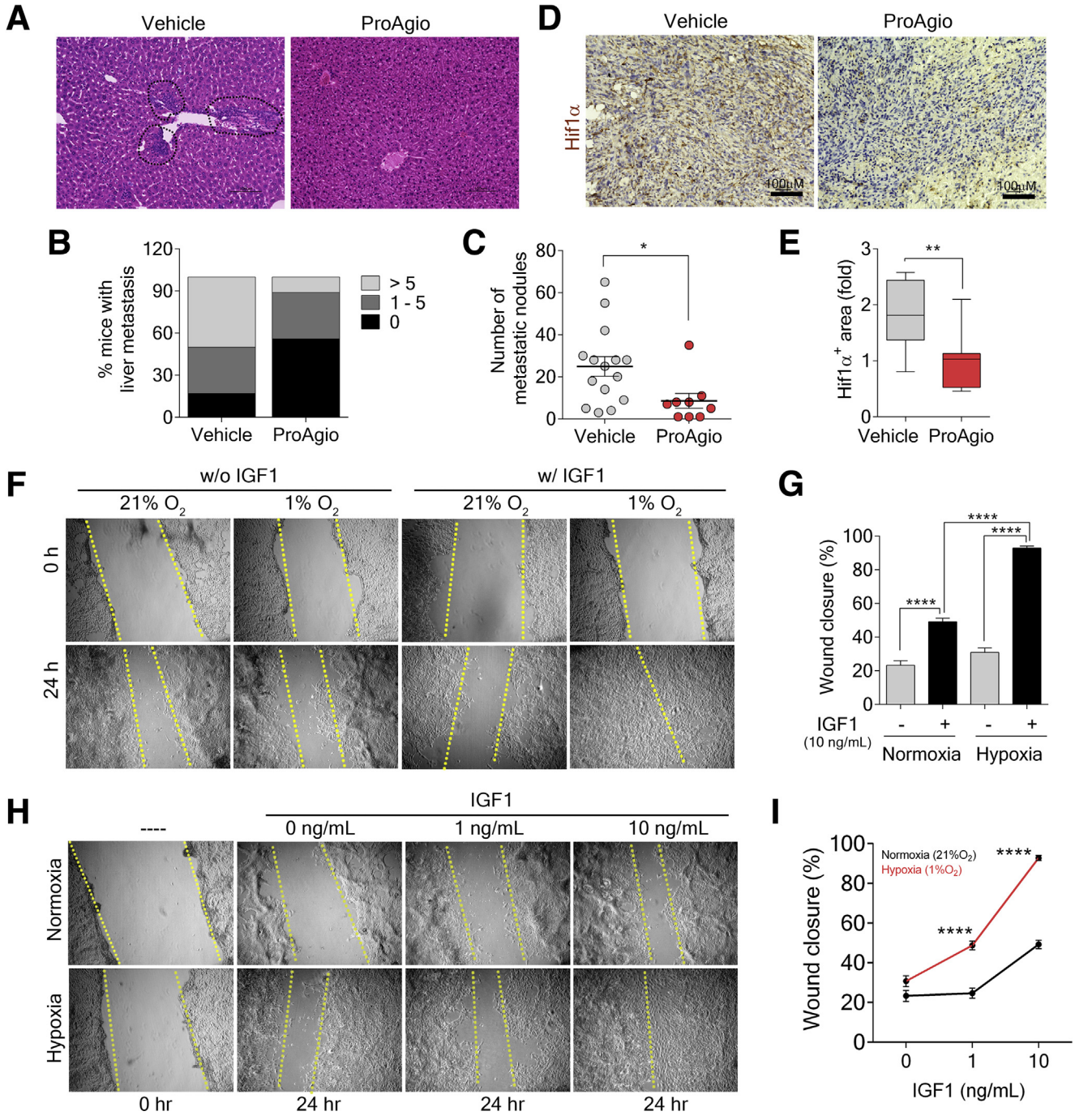

Figure 9. Depletion of CAPaSC by ProAgio decreases metastasis and poorly differentiated tumors. (*A*) Representative images of H&E staining of liver tissue sections of GEM-KPC mice treated with the indicated agents. Liver metastasis lesions were confirmed under the microscope and marked by a *black dotted circle* in the images. (*B* and *C*) Percentage of GEM-KPC mice treated with vehicle or 10 mg/kg ProAgio that show a different number of liver metastatic nodules (>5, >5 nodules; 1–5, 1–5 nodules; 0, no metastatic nodule) (*B*); and the number of metastatic nodules in the liver of GEM-KPC mice treated with vehicle or ProAgio (*C*). Metastatic nodules were assessed by gross inspection of the liver of each treated mouse by naked eye or under the microscope. (*D* and *E*) Representative images of IHC staining of Hif-1α (*D*), and quantitative analyses of Hif-1α stain (*E*, Hif-1α^+ area [fold], fold change by comparison with the mean value of the ProAgio group as 1) in tumor sections of GEM-KPC mice treated with vehicle or ProAgio. (*F* and *G*) In vitro scratch wound healing assay of KPC 961 cells cultured under hypoxia and untreated (*left*) or treated with IGF1 (*right*) compared with those cultured under normoxia as a control (*F*) and quantitative analyses of the migrating cells in the scratched areas (*G*). (*H* and *I*) The scratch wound healing assay of KPC 961 cells cultured under hypoxia and treated with the indicated concentrations of IGF1 for the indicated amounts of time, compared with those cultured under normoxia as a control (*H*) and quantitative analyses of the migrating cells in the scratched areas after IGF1 treatment (*I*). (*G* and *I*) Error bars represent means ± SEM. *$P < .05$, **$P < .01$, ***$P < .001$, ****$P < .0001$. Hif, hypoxia-inducible factor; n.s., denotes not significant.

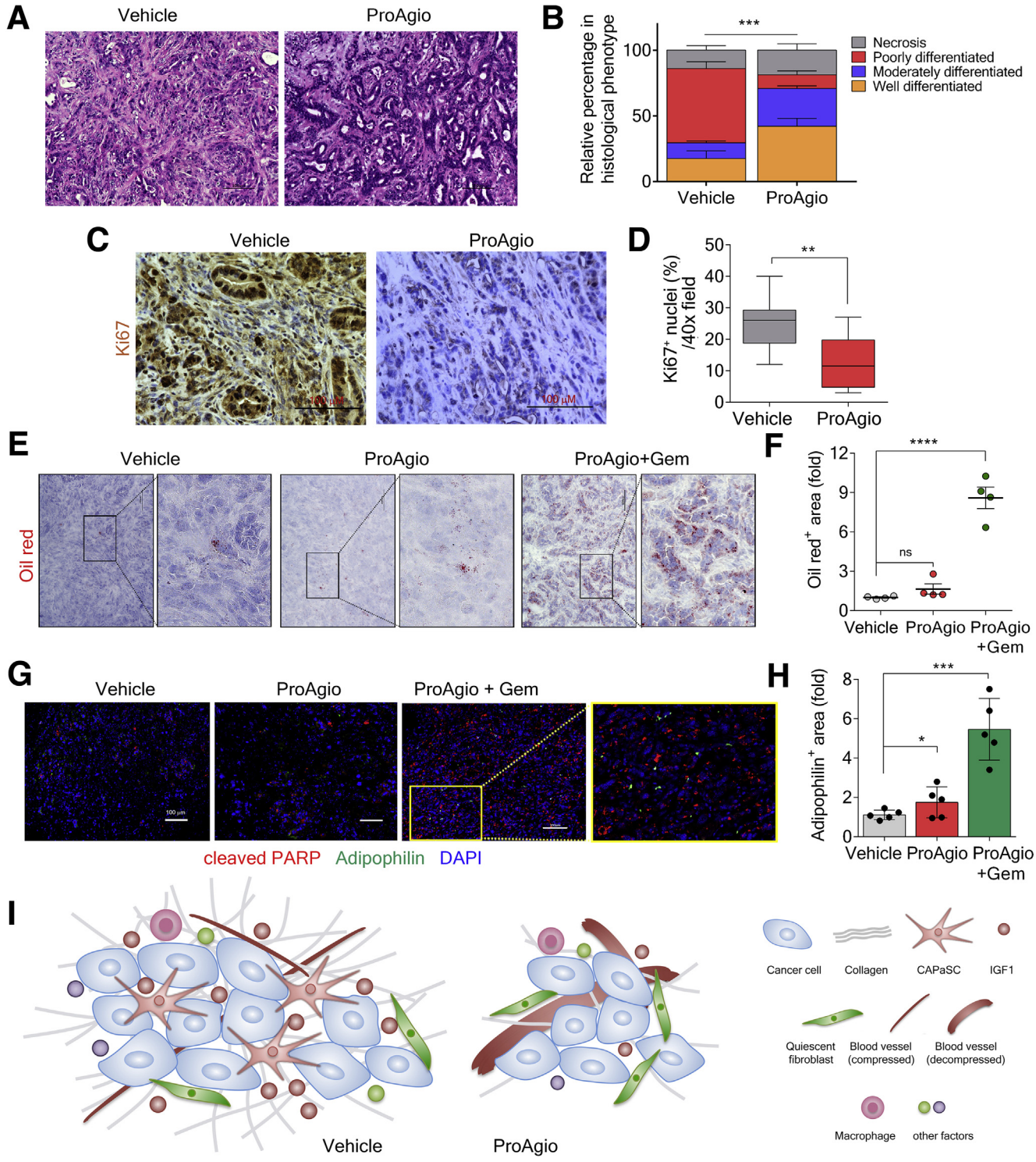

Figure 10. Targeting integrin $\alpha_v\beta_3$ specifically depletes CAPaSC in tumor. (*A* and *B*) Representative images of H&E staining (*A*) and pathologic assessment (*B*) of the tumors of GEM-KPC mice treated with vehicle or ProAgio. (*C* and *D*) Representative images of IHC staining of Ki67 (*C*), and quantitative analyses of Ki67-positive stain area (*D*) in tumor sections of vehicle or ProAgio-treated GEM-KPC mice. (*E* and *F*) Representative images of Oil red O staining (*E*) and quantitative analysis of Oil red O staining (*F*, Oil red$^+$ area [fold], fold change by comparison with the mean value of the vehicle-treated group as 1) in tumor sections of GEM-KPC mice treated with the indicated agents (n = 4). (*G* and *H*) Representative images of co-staining of adipophilin (green) and cleaved PARP (red) (*G*), and quantification of adipophilin stain (*H*, adipophilin$^+$ area [fold], fold change by comparison with the mean value of the vehicle treatment group as 1) in tumor sections of GEM-KPC treated with the indicated agents using ImageJ (n = 5). Image analysis was performed by thresholding for positive staining and normalizing to the total tissue area. Nuclei were stained with 4′,6-diamidino-2-phenylindole (DAPI) (blue). (*I*) Schematic illustration of the mechanism depicting the action of ProAgio in PDAC tumor. (*B*, *F*, and *H*) Error bars represent means ± SEM. PARP, Poly (ADP-ribose) polymerase.

References

1. Olive KP, Jacobetz MA, Davidson CJ, Gopinathan A, McIntyre D, Honess D, Madhu B, Goldgraben MA, Caldwell ME, Allard D, Frese KK, Denicola G, Feig C, Combs C, Winter SP, Ireland-Zecchini H, Reichelt S, Howat WJ, Chang A, Dhara M, Wang L, Rückert F, Grützmann R, Pilarsky C, Izeradjene K, Hingorani SR, Huang P, Davies SE, Plunkett W, Egorin M, Hruban RH, Whitebread N, McGovern K, Adams J, Iacobuzio-Donahue C, Griffiths J, Tuveson DA. Inhibition of Hedgehog signaling enhances delivery of chemotherapy in a mouse model of pancreatic cancer. Science 2009;324:1457–1461.
2. Provenzano PP, Hingorani SR. Hyaluronan, fluid pressure, and stromal resistance in pancreas cancer. Br J Cancer 2013;108:1–8.
3. Provenzano PP, Cuevas C, Chang AE, Goel VK, Von Hoff DD, Hingorani SR. Enzymatic targeting of the stroma ablates physical barriers to treatment of pancreatic ductal adenocarcinoma. Cancer Cell 2012;21:418–429.
4. Hanahan D, Weinberg RA. Hallmarks of cancer: the next generation. Cell 2011;144:646–674.
5. Vonlaufen A, Joshi S, Qu C, Phillips PA, Xu Z, Parker NR, Toi CS, Pirola RC, Wilson JS, Goldstein D, Apte MV. Pancreatic stellate cells: partners in crime with pancreatic cancer cells. Cancer Res 2008;68:2085–2093.
6. Vonlaufen A, Phillips PA, Xu Z, Goldstein D, Pirola RC, Wilson JS, Apte MV. Pancreatic stellate cells and pancreatic cancer cells: an unholy alliance. Cancer Res 2008;68:7707–7710.
7. Eguchi D, Ikenaga N, Ohuchida K, Kozono S, Cui L, Fujiwara K, Fujino M, Ohtsuka T, Mizumoto K, Tanaka M. Hypoxia enhances the interaction between pancreatic stellate cells and cancer cells via increased secretion of connective tissue growth factor. J Surg Res 2013;181:225–233.
8. Ozdemir BC, Pentcheva-Hoang T, Carstens JL, Zheng X, Wu CC, Simpson TR, Laklai H, Sugimoto H, Kahlert C, Novitskiy SV, De Jesus-Acosta A, Sharma P, Heidari P, Mahmood U, Chin L, Moses HL, Weaver VM, Maitra A, Allison JP, LeBleu VS, Kalluri R. Depletion of carcinoma-associated fibroblasts and fibrosis induces immunosuppression and accelerates pancreas cancer with reduced survival. Cancer Cell 2014;25:719–734.
9. Rhim AD, Oberstein PE, Thomas DH, Mirek ET, Palermo CF, Sastra SA, Dekleva EN, Saunders T, Becerra CP, Tattersall IW, Westphalen CB, Kitajewski J, Fernandez-Barrena MG, Fernandez-Zapico ME, Iacobuzio-Donahue C, Olive KP, Stanger BZ. Stromal elements act to restrain, rather than support, pancreatic ductal adenocarcinoma. Cancer Cell 2014;25:735–747.
10. Leake I. Pancreatic cancer: surprising role for fibrosis. Nat Rev Gastroenterol Hepatol 2014;11:396.
11. Catenacci DV, Junttila MR, Karrison T, Bahary N, Horiba MN, Nattam SR, Marsh R, Wallace J, Kozloff M, Rajdev L, Cohen D, Wade J, Sleckman B, Lenz H-J, Stiff, Kumar P, Xu P, Henderson L, Takebe N, Salgia R, Wang X, Stadler WM, de Sauvage FJ, Kindler HL. Randomized phase Ib/II study of gemcitabine plus placebo or vismodegib, a hedgehog pathway inhibitor, in patients with metastatic pancreatic cancer. J Clin Oncol 2015;33:4284–4292.
12. Carr RM, Fernandez-Zapico ME. Pancreatic cancer microenvironment, to target or not to target? EMBO Mol Med 2016;8:80–82.
13. Wilder RL. Integrin alpha V beta 3 as a target for treatment of rheumatoid arthritis and related rheumatic diseases. Ann Rheum Dis 2002;61(Suppl 2):ii96–99.
14. Millard M, Odde S, Neamati N. Integrin targeted therapeutics. Theranostics 2011;1:154–188.
15. Eliceiri BP, Cheresh DA. The role of alphav integrins during angiogenesis: insights into potential mechanisms of action and clinical development. J Clin Invest 1999;103:1227–1230.
16. Turaga RC, Yin L, Yang JJ, Lee H, Ivanov I, Yan C, Yang H, Grossniklaus HE, Wang S, Ma C, Sun L, Liu Z-R. Rational design of a protein that binds integrin alphavbeta3 outside the ligand binding site. Nat Commun 2016;7:11675.
17. Patsenker E, Popov Y, Stickel F, Schneider V, Ledermann M, Sagesser H, Niedobitek G, Goodman SL, Schuppan D. Pharmacological inhibition of integrin alphavbeta3 aggravates experimental liver fibrosis and suppresses hepatic angiogenesis. Hepatology 2009;50:1501–1511.
18. Zhou X, Murphy FR, Gehdu N, Zhang J, Iredale JP, Benyon RC. Engagement of alphavbeta3 integrin regulates proliferation and apoptosis of hepatic stellate cells. J Biol Chem 2004;279:23996–24006.
19. Li F, Song Z, Li Q, Wu J, Wang J, Xie C, Tu C, Wang J, Huang Xiaowei, Lu W. Molecular imaging of hepatic stellate cell activity by visualization of hepatic integrin alphavbeta3 expression with SPECT in rat. Hepatology 2011;54:1020–1030.
20. Erkan M, Reiser-Erkan C, Michalski CW, Kleeff J. Tumor microenvironment and progression of pancreatic cancer. Exp Oncol 2010;32:128–131.
21. Nagy A, Lanczky A, Menyhart O, Gyorffy B. Validation of miRNA prognostic power in hepatocellular carcinoma using expression data of independent datasets. Sci Rep 2018;8:9227.
22. Hingorani SR, Wang L, Multani AS, Combs C, Deramaudt TB, Hruban RH, Rustgi AK, Chang S, Tuveson DA. Trp53R172H and KrasG12D cooperate to promote chromosomal instability and widely metastatic pancreatic ductal adenocarcinoma in mice. Cancer Cell 2005;7:469–483.
23. Tseng WW, Winer D, Kenkel JA, Choi O, Shain AH, Pollack JR, French R, Lowy AM, Engleman EG. Development of an orthotopic model of invasive pancreatic cancer in an immunocompetent murine host. Clin Cancer Res 2010;16:3684–3695.
24. Torres MP, Rachagani S, Souchek JJ, Mallya K, Johansson SL, Batra SK. Novel pancreatic cancer cell lines derived from genetically engineered mouse models of spontaneous pancreatic adenocarcinoma: applications in diagnosis and therapy. PLoS One 2013;8:e80580.
25. Chauhan VP, Boucher Y, Ferrone CR, Roberge S, Martin JD, Stylianopoulos T, Bardeesy N, DePinho RA, Padera TP, Munn LL, Jain RK. Compression of pancreatic tumor blood vessels by hyaluronan is caused by solid stress and not interstitial fluid pressure. Cancer Cell 2014;26:14–15.

26. DelGiorno KE, Carlson MA, Osgood R, Provenzano PP, Brockenbough JS, Thompson CB, Shepard HM, Frost GI, Potter JD, Hingorani SR. Response to Chauhan et al.: interstitial pressure and vascular collapse in pancreas cancer-fluids and solids, measurement and meaning. Cancer Cell 2014;26:16–17.
27. Jia Y, Xie J. Promising molecular mechanisms responsible for gemcitabine resistance in cancer. Genes Dis 2015;2:299–306.
28. Toschi L, Finocchiaro G, Bartolini S, Gioia V, Cappuzzo F. Role of gemcitabine in cancer therapy. Future Oncol 2005;1:7–17.
29. Plunkett W, Huang P, Xu YZ, Heinemann V, Grunewald R, Gandhi V. Gemcitabine: metabolism, mechanisms of action, and self-potentiation. Semin Oncol 1995;22:3–10.
30. Mini E, Nobili S, Caciagli B, Landini I, Mazzei T. Cellular pharmacology of gemcitabine. Ann Oncol 2006;17(Suppl 5):v7–12.
31. Bergman AM, Pinedo HM, Talianidis I, Veerman G, Loves WJ, van der Wilt CL, Peters GJ. Increased sensitivity to gemcitabine of P-glycoprotein and multidrug resistance-associated protein-overexpressing human cancer cell lines. Br J Cancer 2003;88:1963–1970.
32. Ireland L, Santos A, Ahmed MS, Rainer C, Nielsen SR, Quaranta V, Weyer-Czernilofsky U, Engle DD, Perez-Mancera PA, Coupland SE, Taktak A, Bogenrieder T, Tuveson DA, Campbell F, Schmid MC, Mielgo A. Chemoresistance in pancreatic cancer is driven by stroma-derived insulin-like growth factors. Cancer Res 2016;76:6851–6863.
33. Nakano Y, Tanno S, Koizumi K, Nishikawa T, Nakamura K, Minoguchi M, Izawa T, Mizukami Y, Okumura T, Kohgo Y. Gemcitabine chemoresistance and molecular markers associated with gemcitabine transport and metabolism in human pancreatic cancer cells. Br J Cancer 2007;96:457–463.
34. Laron Z. Insulin-like growth factor 1 (IGF-1): a growth hormone. Mol Pathol 2001;54:311–316.
35. Werner H, Bruchim I. Basic and clinical significance of IGF-I-induced signatures in cancer. BMC Med 2010;8:2.
36. Hirakawa T, Yashiro M, Doi Y, Kinoshita H, Morisaki T, Fukuoka T, Hasegawa T, Kimura K, Amano R, Hirakawa K. Pancreatic fibroblasts stimulate the motility of pancreatic cancer cells through IGF1/IGF1R signaling under hypoxia. PLoS One 2016;11:e0159912.
37. Gascard P, Tlsty TD. Carcinoma-associated fibroblasts: orchestrating the composition of malignancy. Genes Dev 2016;30:1002–1019.
38. Korc M. Pancreatic cancer-associated stroma production. Am J Surg 2007;194:S84–S86.
39. Joung YH, Lee MY, Lim EJ, Kim MS, Hwang TS, Kim SY. Hypoxia activates the IGF-1 expression through STAT5b in human HepG2 cells. Biochem Biophys Res Commun 2007;358:733–738.
40. Villanueva J, Vultur A, Lee JT, Somasundaram R, Fukunaga-Kalabis M, Cipolla AK, Wubbenhorst B, Xu X, Gimotty PA, Kee Damien, Santiago-Walker AE, Letrero R, D'Andrea K, Pushparajan Anitha, Hayden JE, Dahlman Brown K, Laquerre S, McArthur GA, Sosman JA, Nathanson KL, Herlyn M. Acquired resistance to BRAF inhibitors mediated by a RAF kinase switch in melanoma can be overcome by cotargeting MEK and IGF-1R/PI3K. Cancer Cell 2010;18:683–695.
41. Nielsen MFB, Mortensen MB, Detlefsen S. Identification of markers for quiescent pancreatic stellate cells in the normal human pancreas. Histochem Cell Biol 2017;148:359–380.
42. Ligorio M, Sil S, Malagon-Lopez J, Nieman LT, Misale S, Di Pilato M, Ebright RY, Karabacak MN, Kulkarni AS, Liu A, Vincent Jordan N, Franses JW, Philipp J, Kreuzer J, Desai N, Arora KS, Rajurkar M, Horwitz E, Neyaz A, Tai E, Magnus NKC, Vo KD, Yashaswini CN, Marangoni F, Boukhali M, Fatherree JP, Damon LJ, Xega K, Desai R, Choz M, Bersani F, Langenbucher A, Thapar V, Morris R, Wellner UF, Schilling O, Lawrence MS, Liss AS, Rivera MN, Deshpande V, Benes CH, Maheswaran S, Haber DA, Fernandez-Del-Castillo C, Ferrone CR, Haas W, Aryee MJ, Ting DT. Stromal microenvironment shapes the intratumoral architecture of pancreatic cancer. Cell 2019;178:160–175.e27.
43. Hessmann E, Patzak MS, Klein L, Chen N, Kari V, Ramu I, Bapiro TE, Frese KK, Gopinathan A, Richards FM, Jodrell DI, Verbeke C, Li X, Heuchel R, Löhr JM, Johnsen SA, Gress TM, Ellenrieder V, Neesse A. Fibroblast drug scavenging increases intratumoural gemcitabine accumulation in murine pancreas cancer. Gut 2018;67:497–507.

Received February 7, 2020. Accepted August 12, 2020.

Correspondence
Address correspondence to: Zhi-Ren Liu, PhD, Department of Biology, Georgia State University, University Plaza, Atlanta, Georgia 30303. e-mail: zliu8@gsu.edu; fax: (404) 413-5300.

Acknowledgments
The authors thank Bassel El-Rayes, Christine Alewine, Gregory Lesinski, David Tuveson, Robert B. Diasio, Thomas M. Roberts, and Liangwei Li for the useful suggestions and comments on the manuscript. The authors thank Mukkavilli Rao for help in quantification of gemcitabine and its metabolites. The authors are grateful to Chengliu Jin and Qian Liu for their help in GEMKPC mice breeding.

CRediT Authorship Contributions
Zhi-Ren Liu, PhD (Conceptualization: Lead; Formal analysis: Lead; Funding acquisition: Lead; Investigation: Lead; Project administration: Lead; Supervision: Lead; Writing – original draft: Lead; Writing – review & editing: Lead);

Ravi Chakra Turaga, PhD (Data curation: Equal; Formal analysis: Equal; Investigation: Equal; Methodology: Equal; Supporting: study plan);

Malvika Sharma, MS (Data curation: Equal; Formal analysis: Equal; Investigation: Equal; Methodology: Equal);

Falguni Mishra, BS (Investigation: Supporting; Methodology: Supporting);

Alyssa Krasinskas, MD (Formal analysis: Supporting; Methodology: Supporting; Resources: Supporting);

Yi Yuan, MS (Investigation: Supporting; Methodology: Supporting);

Jenny Yang, PhD (Formal analysis: Supporting; Funding acquisition: Supporting; Methodology: Supporting);

Shiyuan Wang, PhD (Investigation: Supporting; Resources: Supporting);

Chunfeng Liu, PhD (Investigation: Supporting; Resources: Supporting);

Li Sun, PhD (Formal analysis: Supporting; Investigation: Supporting; Resources: Supporting).

Conflicts of interest
These authors disclose the following: Zhi-Ren Liu holds shares in ProDa BioTech LLC, which licensed the rights to commercialize ProAgio; and Sun Li holds shares in Amoytop Biotech Co, Ltd, which licensed the rights to commercialize ProAgio in China. The remaining authors disclose no conflicts.

Funding
This work is supported in part by research grants from the National Institutes of Health (CA175112, CA118113, CA178730, and CA217482) and the Georgia Cancer Coalition (Z.-R.L.); and by a Molecular Basis of Disease fellowship, Georgia State University (R.C.T. and M.S.).